The acetylase activity of Cdu1 regulates bacterial exit from infected cells by protecting *Chlamydia* effectors from degradation

Robert J. Bastidas[1*], Mateusz Kędzior[1], Robert K. Davidson[2,#], Stephen C. Walsh[2,#], Lee Dolat[1], Barbara S. Sixt[3,4,5], Jonathan N. Pruneda[6] , Jörn Coers[1,2], Raphael H. Valdivia[1,2*]

Author affiliations: [1]Department of Integrative Immunobiology, Duke University, Durham, N.C 27708, USA. [2]Department of Molecular Genetics and Microbiology, Duke University, Durham, N.C 27708, USA. [3]Deparment of Molecular Biology, Umeå University, Umeå, Sweden. [4]The Laboratory for Molecular Infection Medicine Sweden (MIMS), Umeå University, Umeå, Sweden. [5]Umeå Centre for Microbial Research (UCMR), Umeå University, Umeå, Sweden. [6]Department of Molecular Microbiology & Immunology, Oregon Health & Science University, Portland, OR 97239, USA. [#]Authors contributed equally.

* Correspondence: robert.bastidas@duke.edu; raphael.valdivia@duke.edu

Abstract

Many cellular processes are regulated by ubiquitin-mediated proteasomal degradation. Pathogens can regulate eukaryotic proteolysis through the delivery of proteins with de-ubiquitinating (DUB) activities. The obligate intracellular pathogen *Chlamydia trachomatis* secretes Cdu1 (ChlaDUB1), a dual deubiquitinase and Lys-acetyltransferase, that promotes Golgi remodeling and survival of infected host cells presumably by regulating the ubiquitination of host and bacterial proteins. Here we determined that Cdu1's acetylase but not its DUB activity is important to protect Cdu1 from ubiquitin-mediated degradation. We further identified three *C. trachomatis* proteins on the pathogen-containing vacuole (InaC, IpaM, and CTL0480) that required Cdu1's acetylase activity for protection from degradation and determined that Cdu1 and these Cdu1-protected proteins are required for optimal egress of *Chlamydia* from host cells. These findings highlight a non-canonical mechanism of pathogen-mediated protection of virulence factors from degradation after their delivery into host cells and the coordinated regulation of secreted effector proteins.

Introduction

Ubiquitination is a conserved and ubiquitous post-translational modification (PTM) of proteins involving the conjugation of the carboxy-terminal glycine residue of ubiquitin (Ub) to lysine residues of target proteins. Poly-ubiquitination of substrates involves further conjugation of a Ub internal lysine residue or amino-terminal methionine (M1) with a second Ub molecule. Seven internal lysines in Ub (K6, K11, K27, K29, K33, K48, K63) and M1 are utilized by Ub conjugating enzymes to form homogeneous, branched, or mixed poly-ubiquitin (polyUb) chains (Komander and Rape., 2012). PolyUb chains with different linkage types exhibit distinct structures and functions. For example, K48- and K11-linked polyUb chains exhibit a compact conformation and are substrates for 26S proteasome-mediated degradation (Varadan et al., 2004; Tenno et al., 2004; Eddins et al., 2007; Bremm et al., 2010; Saeki., 2017). In contrast, K63-linked polyUb

conjugates adopt more open conformations that enable the recruitment of multiprotein complexes that regulate the function of the target protein by proteolytic independent events (Komander et al., 2009b; Weeks et al., 2009; Datta et al., 2009; Komander and Rape., 2012). Mixed and branched polyUb chains are also emerging as important regulators of physiological functions (Swatek and Komander., 2016; Ohtake and Tsuchiya., 2017).

Protein ubiquitination regulates numerous eukaryotic cell processes including protein degradation, signal transduction, cell cycle regulation, selective autophagy, the DNA damage response, and programmed cell death. Ub also plays key roles in modulating host innate immune responses to bacterial infection (Li et al., 2016), bacterial proteins, pathogen-containing vacuoles, and bacteria themselves by targeting them for Ub-mediated degradation by proteasomal or autophagic machineries (Li et al., 2016). Because the Ub system is critical for pathogen containment, many pathogens have evolved mechanisms to counteract the impact of this PTM (Vozandychova et al., 2021). For instance, bacterial deubiquitinases (DUBs) can remove Ub from ubiquitinated substrates thereby dampening inflammatory and cell-autonomous defense mechanisms (Kubori et al., 2019). Many DUBs are cysteine proteases with a catalytic Cys, a nearby His and an Asn/Asp (Komander et al., 2009a). DUBs are typically dedicated to the removal of Ub moieties and are unable to hydrolyze other Ub-like (Ubl) modifications such as SUMO or NEDD8. However, the CE clan of Ubl proteases (ULPs) can catalyze the removal of both SUMO and NEDD8 (Ronau et al., 2016). Bacterial pathogens also encode CE clan enzymes that function as DUBs, ULPs or both. For instance, *Salmonella* Typhimurium SseL, *Escherichia coli* ElaD, and *Shigella flexneri* ShiCE function as Ub specific proteases (Rytkönen et al., 2007; Catic et al., 2007; Pruneda et al., 2016) while RickCE from *Rickettsia belli* functions as a protease directed towards both Ub and NEDD8 as does SidE from *Legionella pneumophila* which displays mixed activities towards Ub, NEDD8, and ISG15 (Sheedlo et al., 2015; Pruneda et al., 2016). Similarly, XopD from *Xanthamonas campestris* and LotB from *L. pneumophila* are

isopeptidases exhibiting cross reactivity towards both Ub and SUMO (Pruneda et al., 2016; Schubert et al., 2020). Some CE clan bacterial effectors display acetyltransferase activity. *L. pneumophila* LegCE, *S.* Typhimurium AvrA, and YopJ from *Yersinia pestis* function exclusively as acetyltransferases (Mittal et al., 2006; Mukherjee et al., 2006; Jones et al., 2008; Pruneda et al., 2016). In contrast, the *Chlamydia trachomatis* (Ct) effector Cdu1/*Chla*DUB1 is a CE clan protein that exhibits both acetyltransferase and deubiquitinating activities (Misaghi et al., 2006; Pruneda et al., 2016; Fischer et al., 2017; Pruneda et al., 2018).

Ct is an obligate intracellular bacterial pathogen responsible for human diseases of significant clinical and public health importance (Haggerty et al., 2010). Ct has a biphasic developmental cycle in which the Ct infectious propagule or elementary body (EB) invades the target host cell. Upon internalization the EB transitions to the reticulate body (RB). RBs replicate by binary fission within a pathogenic vacuole ("inclusion") and asynchronously differentiate back to EBs. In cell culture, starting at around 48 hours-post infection (hpi) Ct will egress after lysis of the host cell or by a process termed extrusion, wherein the intact inclusion exits from the infected cell (Moulder., 1991; Abdelrahman and Belland., 2005; Hybiske and Stephens., 2007; Lee et al., 2018). The effector Cdu1 was originally identified as a deneddylating and deubiquitinating enzyme and subsequently shown to exhibit *in-vitro* isopeptidase activity towards both Lys48 and Lys63 linked di-Ub substrates (Misaghi et al., 2006; Claessen et al., 2013; Pruneda et al., 2016; Fischer et al., 2017). Cdu1 is unique among CE clan enzymes in that it also functions as a bona fide lysine acetylase with both is acetylase and DUB activities catalyzed by the same catalytic active site (Pruneda et al., 2018). Intriguingly, Cdu1 autoacetylation is directed towards lysines unlike other CE clan acetylases that predominantly target serine and threonine residues (Pruneda et al., 2018). In transfected cells, Cdu1 protects the NFκB cytoplasmic retention factor IκBα from ubiquitination and proteasomal degradation (Le Negrate et al., 2008). In infected

cells, Cdu1 localizes to the inclusion membrane where it functions to stabilize the anti-apoptotic protein Mcl-1 and to promote the repositioning of Golgi ministacks around the Ct inclusion (Fischer et al., 2017; Wang et al., 2018; Pruneda et al., 2018; Kunz et al., 2019; Auer et al., 2020). However, the mechanism by which Cdu1 promotes redeployment of Golgi ministacks and any additional roles that Cdu1 may play during Ct infection of epithelial cells remains unknown.

In this study, we show that Cdu1 protects itself and three secreted Ct effectors, InaC, IpaM, and CTL0480 from targeted ubiquitination and proteasomal degradation. InaC, IpaM, and CTL0480 are members of a larger family of bacterial proteins embedded within the inclusion membrane (Inc proteins) (Bannantine et al., 2000; Rockey et al., 2002; Chen et al., 2006; Li et al., 2008; Alzhanov et al., 2009; Dehoux et al., 2011; Lutter et al., 2012; Lutter et al., 2013; Kokes et al., 2015; Weber et al., 2015). We show that Cdu1-mediated protection from degradation is independent from its DUB activity but relies upon its Lys acetylase activity. We show that Cdu1 protects InaC to promote repositioning of Golgi ministacks and formation of actin scaffolds around the Ct inclusion, and CTL0480 to promote recruitment of myosin phosphatase target subunit 1 (MYPT1) to the inclusion. In addition, we determined that Cdu1 and Cdu1-protected Incs are required for optimal extrusion of inclusions from host cells at the late stages of infection.

Results

The *C. trachomatis* inclusion membrane proteins InaC, IpaM, and CTL0480 are differentially ubiquitinated in the absence of Cdu1

Cdu1 is required for Golgi repositioning around the Ct inclusion (Pruneda et al., 2018; Auer et al., 2020). To understand how Cdu1 promotes Golgi redistribution, we first generated a *cdu1*

null strain in a Ct L2 background by TargeTron mediated insertional mutagenesis (pDFTT3-*aadA*) (Lowden et al., 2015) (S. Figure 1). Loss of Cdu1 expression in the resulting L2 *cdu1*::GII *aadA* (*cdu1*::GII) strain was verified by western blot analysis and by indirect immunofluorescence with antibodies raised against Cdu1 (S. Figures 2A and 2B). Because *cdu2* resides directly downstream of the *cdu1* locus and encodes a second Ct DUB (Cdu2/*Chla*DUB2) (Misaghi et al., 2006), we first determined whether the disruption of *cdu1* impacted the expression of *cdu2*. We detected *cdu1* and *cdu2* transcripts in HeLa cells infected with Ct L2 but not for the juncture between *cdu1* and *cdu2* (S. Figure 2C). In cells infected with Ct *cdu1*::GII we only detected *cdu2* transcripts (S. Figure 2C) confirming that *cdu1* and *cdu2* are not co-expressed as part of an operon in accordance with previous observations (Albrecht et al., 2010).

In transfected Hela cells, Cdu1's DUB activity has been linked to fragmentation of the Golgi apparatus (Pruneda et al., 2018). We therefore hypothesized that Cdu1s' DUB activity in infected cells promoted Golgi redistribution around inclusions and that we could identify potential targets by comparing the protein ubiquitination profile of cells infected with WT or *cdu1*::GII strains by quantitative mass spectrometry (MS). HeLa cell were mock infected or infected with either WT L2 or *cdu1*::GII strains. At 24 hpi, poly-ubiquitinated proteins were enriched from lysed cells using Tandem Ubiquitin Binding Entities (TUBEs) (LifeSensors). TUBEs consist of concatenated Ub binding associated domains (UBAs) that bind to polyUb-modified proteins with nanomolar affinities. Poly-ubiquitinated proteins of both human and Ct origin were enriched and identified by quantitative LC-MS/MS analysis.

Over 2,000 non-ubiquitinated proteins co-precipitated with TUBE 1 bound proteins across all three conditions (mock, L2, and *cdu1*::GII infected HeLa cells) and 3 biological replicates (S. Table 1). Among these, 47 human proteins were significantly enriched in mock infected HeLa

cells and 50 human proteins were significantly enriched during Ct infection (L2 and *cdu1*::GII) (S. Table 3, S. Figure 3) Pathway enrichment analysis revealed that proteins involved in RNA metabolism were overrepresented among co-precipitating proteins from mock infected cells (S. Table 4, S. Figure 4) while no biological pathways or processes were overrepresented in proteins enriched from infected cells (S. Figure 4). We also identified 8 TUBE1 co-precipitating Ct proteins in HeLa cells infected with L2 and *cdu1*::GII (S. Table 5, S. Figure 3).

TUBE 1 affinity capture lead to the identification of 43 ubiquitinated proteins (35 human proteins and 8 Ct proteins across all 3 conditions and replicates) based on the presence of peptides containing a di-glycine remnant motif (Peng et al., 2003) (S. Tables 6-8). The lack of widespread poly-ubiquitination of either human or Ct proteins in response to Ct infection (Figure 1) was surprising given that wholesale changes in protein ubiquitination has been reported during infection of HeLa cells by intracellular pathogens like *S.* Typhimurium (Fiskin et al., 2016). It is also possible that had we conducted our analysis at different time points post-infection (hpi), we might have identified additional Cdu1 targets, such as Mcl1 and IκBα (Le Negrate et al., 2008; Fischer et al., 2017) which were not identified in our analysis. However, given that we observed Cdu1 at the inclusion membrane as early as 1 hpi (data not shown), we opted to focus on an earlier stage of the infection cycle. Only two human ubiquitinated proteins (ZC3H7A and DDIT4) were found to be significantly enriched in response to WT L2 infection at 24 hpi (Figures 1A and 1C, S. Table 8) while only one human protein (MGC3121) was preferentially ubiquitinated in HeLa cells infected with the *cdu1*::GII mutant strain (Figures 1B and 1C, S. Table 8). In contrast three Ct proteins, InaC (K104, K107, and K149), IpaM (K29), and CTL0480 (K115) were ubiquitinated at Lys residues in the absence of Cdu1 (Figures 1B, 1C, and 1D, S. Table 8).

InaC, IpaM, and CTL0480 are Ct effector proteins that localize to the inclusion membrane (Chen et al., 2006; Alzhanov et al., 2009; Lutter et al., 2013; Kokes et al., 2015). These Type 3

secretion substrates belong to a family of over 36 inclusion membrane proteins (Incs) that contain a signature bi-lobal hydrophobic transmembrane domain (Bannantine et al., 2000; Rockey et al., 2002; Li et al., 2008; Dehoux et al., 2011; Lutter et al., 2012). Incs provide many functions important for Ct intracellular replication ranging from providing structural integrity to the inclusion membrane, to regulating membrane trafficking, to mediating interactions with host organelles and cytoskeletal structures (reviewed in Bugalhão et al., 2019). InaC facilitates the activation of the small GTPase RhoA, a crucial step for the assembly of actin scaffolds around the inclusion (Haines et al., 2021; Kumar and Valdivia., 2008). Additionally, InaC plays a pivotal role in the activation of Arf GTPases. This activation subsequently induces post-translational modifications of microtubules in close proximity to the inclusion membrane, which are essential for Ct to initiate the repositioning of Golgi ministacks around the inclusion (Wesolowski et al., 2017). IpaM exhibits localization to discrete patches in the inclusion termed microdomains (Alzhanov et al., 2009; Dumoux et al., 2015). Upon ectopic expression, IpaM induces alterations in microtubule organization (Dumoux et al., 2015). CTL0480, facilitates the recruitment of MYPT1 (myosin phosphatase target subunit 1) to the inclusion membrane. Recrutiment of MYPT1 is required for the efficient exit of Ct from host cells (Lutter et al., 2013; Shaw et al., 2018). Because Cdu1 also localizes to the inclusion membrane (Fischer et al., 2017; Wang et al., 2018; Pruneda et al., 2018; Kunz et al., 2019) we postulated that Cdu1 directly protects InaC, IpaM, and CTL0480 from ubiquitination.

Cdu1 associates with InaC, IpaM, and CTL0480

We first determined if Cdu1 co-localized with InaC, IpaM, and CTL0480 at the inclusion membrane. HeLa cells were infected for 24 hours with WT L2 or L2 expressing CTL0480-Flag from its endogenous promoter and immunostained with antibodies against Cdu1, InaC, IpaM, or the Flag epitope. Both InaC and CTL0480-Flag localized throughout the inclusion membrane while IpaM was restricted to discrete microdomains as previously reported (Alzhanov et al.,

2009; Dumoux et al., 2015) (Figure 2A). Cdu1 co-localized with InaC and CTL0480-Flag and with IpaM at microdomains (Figures 2A and 2B). All four antibodies specifically recognized their corresponding antigens since immunostaining for Cdu1, InaC, IpaM or the Flag epitope was not observed in Ct strains lacking Cdu1 (*cdu1*::GII), InaC (M407, Kokes et al., 2015) IpaM (*ipaM*::GII, Meier et al., 2022), or a strain that does not express CTL0480-Flag (Figure 2A).

We next determined if Cdu1 can interact with InaC, IpaM, and CTL0480 by co-transfecting HEK 293 cells with vectors expressing either full length Cdu1-GFP or truncated versions of Cdu1-GFP lacking transmembrane or catalytic domains (Figure 2C), and vectors expressing Flag-InaC, V5-IpaM, and V5-CTL0480. Transfected cells were lysed and Cdu1-GFP was immunoprecipitated with antibodies against GFP. Western blot analysis of the immunoprecipitates showed that Flag-InaC, V5-IpaM, and V5-CTL0480 co-precipitated with Cdu1-GFP (Figures 2D-F). Moreover, the transmembrane domain of Cdu1 was necessary for Cdu1-GFP to interact with all three Incs (Figures 2D-F). The interaction between Cdu1-GFP and the three tagged Incs was specific since we did not detect interactions between Cdu1-GFP and a V5-tagged version of the inclusion membrane protein CpoS (Sixt et al., 2017) (Figure 2G). We expected these interactions to be transient at the inclusion membrane as the engagement of Cdu1 with its target(s) should mimic that of most enzymes with their substrates. Therefore, while we could capture these complexes in co-immunoprecipitations in the context of overexpression, this assay was not sensitive enough to reliably document the formation of complexes among low abundance endogenous Ct proteins. Nevertheless, our findings from transfection experiments lead us to conclude that Cdu1 can selectively interact with all three Incs even in the absence of infection, and these interactions are facilitated by the transmembrane domain of Cdu1.

Cdu1 protects InaC, IpaM, and CTL0480 proteins from degradation during infection

We next assessed if Cdu1 was required to stabilize endogenous InaC, IpaM, and CTL0480 in infected cells. HeLa cells were infected with either WT L2 or *cdu1*::GII strains and at various time points in the Ct infectious cycle crude cell lysates were analyzed by western blot to assess the relative abundance of Inc proteins. At 36 and 48 hpi, the levels of InaC protein were found to be undetectable in cells infected with *cdu1*::GII in comparison to cells infected with the WT L2 strain (Figures 3A and 3B). Conversely, IpaM protein levels exhibited a decrease at 36 and 48 hpi in cells infected with *cdu1*::GII (Figure 3C and 3D). We were not able to detect CTL0480 levels by western blot but were successful in following CTL0480 expression by indirect immunofluorescence (Figure 3E). The relative abundance of CTL0480 at inclusion membranes was not affected in *cdu1*::GII inclusions at 24 hpi. However, at 36 hpi, a subpopulation of cells lost CTL0480 immunoreactivity and by 48 hpi, inclusion membranes of the *cdu1*::GII strain were devoid of CTL0480 while CTL0480 was prominently detected at the inclusion membranes of WT L2 (Figures 3E and Supplemental Figure 5). As controls for the specificity of antibodies used for western blots and for indirect immunofluorescence, we included cells infected with Ct lacking *ipaM (ipaM*::GII, Meier et al., 2022), with an *inaC* nonsense mutant (M407, Kokes et al., 2015), and with Ct lacking *ctl0480* (*ctl0480*::GII, Shaw et al., 2018). Overall, our results indicate that steady state protein levels of InaC and IpaM and CTL0480 localization at the inclusion membrane, especially at late stages of infection, are dependent on Cdu1, and that Cdu1 acts at different stages in the infection cycle.

The acetylase activity of Cdu1 is required for Cdu1 to protect itself, InaC, and IpaM from polyubiquitination and proteasomal degradation

The crystal structures of Cdu1 bound to Ub or Coenzyme A indicated that the adenosine and phosphate groups of Coenzyme A make contact with a helix in variable region 3 (VR-3) of Cdu1 while the Ile36-patch of Ub binds to the opposite face of the same helix (Pruneda et al., 2018).

Although Cdu1 catalyzes both of its DUB and acetylase (Act) activities with the same active site (Pruneda et al., 2018) the two activities of Cdu1 can be uncoupled by the amino acid substitution K268E in VR-3 which disrupts Coenzyme A binding required for Act activity and by the amino acid substitution I225A in the Ub-binding region of VR-3 required for DUB activity (Pruneda et al., 2018). These substitutions allowed us to test which of Cdu1's enzymatic functions are required for the observed effects on protein stability. We generated Ct shuttle plasmids, expressing WT Cdu1, a catalytically inactive variant of Cdu1 lacking both DUB and Act activities (Cdu1^{C345A}) (Pruneda et al., 2018), a Cdu1 DUB-deficient variant (Cdu1^{I225A}), and a Cdu1 Act-deficient variant (Cdu1^{K268E}). All Cdu1 constructs were expressed from the *cdu1* endogenous promoter as 3X Flag epitope-tagged proteins.

Plasmids expressing each Cdu1 variant were transformed into the *cdu*1::GII mutant and the resulting strains used to infect HeLa cells for 36 and 48 hours. The levels of endogenous InaC and IpaM in cell extracts of infected cells were monitored by western blot analysis. At 36 hpi, InaC protein levels drastically decreased in cells infected with *cdu1* null strains transformed with empty vector or expressing the catalytic inactive variant of Cdu1 (Cdu1^{C345A}-Flag) (Figure 4A). Likewise, IpaM protein levels diminished at 48 hpi during infection with the same strains (Figure 4B). Both InaC and IpaM protein levels were restored to wild type levels in *cdu1* null strains complemented with wild type Cdu1-Flag (Figures 4A and 4B). Unexpectedly, cells infected with a *cdu1* null strain ectopically expressing the DUB deficient Cdu1 variant (Cdu1^{I225A}-Flag) displayed wild type levels of InaC and IpaM while the Act deficient variant (Cdu1^{K268E}-Flag) did not (Figures 4A and 4B). These results suggest that the acetylase activity of Cdu1 rather than its DUB activity is required for Cdu1's ability to stabilize InaC and IpaM proteins.

When we monitored the stability of each Flag-tagged Cdu1 variant, we observed that the catalytically inactive variant of Cdu1 (C345A-Flag) was destabilized (Figures 4A and 4B- Flag WB). We reasoned that Cdu1 also protects itself from being targeted for degradation in infected cells. As with InaC and IpaM, the acetylase but not the DUB activity of Cdu1 was required for Cdu1's stability (Figures 4A and 4B). Although the C345A (DUB-, Act-) and K268E (Act-) amino acid substitutions in Cdu1 do not destabilize Cdu1 expressed in *E. coli* (Pruneda et al., 2018), it was possible that these substitutions impacted the expression and/or folding of Cdu1 in *Chlamydia*. To determine if these Cdu1 mutants were inherently unstable, we expressed Cdu1^{C345A}-Flag and Cdu1^{K268E}-Flag in WT L2 in the presence of endogenous Cdu1. We found that each Flag-tagged variant was stabilized (Figure 4C), indicating that endogenous Cdu1 protected the catalytically-deficient Cdu1 variants *in trans*. In addition, western blot analysis of immunoprecipitated Cdu1-Flag and Cdu1^{C345A}-Flag expressed in a *cdu1*::GII mutant showed that while WT Cdu1-Flag was not modified by Lys48-linked poly-ubiquitination, Cdu1^{C345A}-Flag was robustly modified by Lys48-linked polyUb in the presence of the proteasome inhibitor MG132 (Figure 4D). Moreover, endogenous Cdu1 protected Cdu1^{C345A}-Flag from Lys48-linked polyUb when Cdu1^{C345A}-Flag was expressed in a wild type L2 background (Figure 4D). These results indicate that the loss of Cdu1 activity likely leads to its Lys48-linked poly-ubiquitination and subsequent proteasome-dependent degradation.

Because Cdu1 autoacetylates itself and its Act activity is directed towards lysines (Pruneda et al., 2018) we postulated that Cdu1 may stabilize proteins from degradation by acetylating lysine residues that are potential targets of ubiquitination. We tested this hypothesis by assessing whether Cdu1, InaC, CTL0480, and IpaM are acetylated at lysines during infection. Fractions enriched for inclusion membranes were isolated by sub-cellular fractionation from HeLa cells

infected with wild-type L2 (24 hpi), and proteins acetylated at lysines were immunoprecipitated. Western blot analysis of acetyl-lysine immunoprecipitates indicated that InaC and IpaM, but not the Inc protein IncA, were acetylated (Figure 4E). Western blot analysis of anti-acetyl-lysine immunoprecipitates of inclusion membrane-enriched membrane fractions of HeLa cells infected with L2 expressing Cdu1-Flag (24 hpi), CTL0480-Flag (40 hpi), and IpaM-Flag (40 hpi) also showed that all three Flag tagged effectors were acetylated at lysines (Figure 4F). We also determined that Flag-tagged InaC expressed in an *inaC* null (M407) background was acetylated at lysines as determined by western blot analysis of anti-acetyl-lysine immunoprecipitates (Figure 4G). In addition, we identified acetylated forms of Cdu1 from mass spectrometric analysis of Flag immunoprecipitates derived from extracts of HeLa cells infected with L2 expressing Cdu1-Flag, (24 hpi) (Figure 4H).

Cdu1's acetylase activity shields inclusions from ubiquitination but is not sufficient to protect against IFNγ mediated antimicrobial activity.

We reasoned that the lysine acetylase activity of Cdu1 is a prominent mechanism by which Cdu1 protects client proteins (at 24 hpi), since loss of Cdu1 or expression of the acetylase deficient variant of Cdu1 (Cdu1^{K268E}-Flag) leads to a marked increase in Ub immunostaining at or near the periphery of *cdu1*::GII inclusions (> 80% of inclusions) compared to HeLa cells infected with *cdu1*::GII strains complemented with wild type or DUB deficient (I225A-Flag) Cdu1 strains (Figures 5A, 5B, and Supplemental Figure 6A). Given that Cdu1 appears to localize exclusively at inclusion membranes we predicted that its activity would be spatially restricted to the inclusion periphery. We tested this premise by co-infecting HeLa cells with an *incA* null strain (M923 (IncA^{R197*}), Kokes et al., 2015) and the *cdu1*::GII strain. IncA mediates homotypic fusion of inclusion membranes and loss of IncA results in the accumulation of multiple unfused inclusions in cells infected at high MOIs (Hackstadt et al., 1999; Suchland et

al., 2000; Pannekoek et al., 2005) (Figure 5C). As expected, *incA* mutants which retain Cdu1 activity did not accumulate Ub at or near the periphery of inclusion membranes. In HeLa cells coinfected with both *cdu1*::GII and M923 (IncA^{R197*}), *cdu1::GII* Cdu1^{C345A} and M923, or *cdu1*::GII Cdu1^{K268E} and M923, only the *incA* null inclusions were protected from ubiquitination (Figures 5C, 5D, and Supplemental Figure 6B). Based on these observations we conclude that the acetylase activity of Cdu1 protects proteins *in cis* and that this activity is constrained to the membrane of the pathogenic vacuole consistent with previous reports (Auer et al., 2020).

Recently, the Ct inclusion membrane protein GarD was identified as a Ct effector that shields Ct from γ-interferon mediated ubiquitination by the IFNγ-inducible human ubiquitin E3 ligase RNF213 (Walsh et al., 2022). Because Cdu1 also protects the Ct inclusion from ubiquitination, we tested if Cdu1 also plays a role in protecting Ct from IFNγ-induced cell immunity. A549 cells were pretreated with IFNγ (100 U/mL) and infected with WT Ct, *cdu1*::GII, or *garD*::GII strains. Infections with a *garD*::GII strain led to an approximate 90% decrease in the number of inclusions formed relative to infections with its parental WT Ct strain (Figure 5E) while infections with a *cdu1*::GII or its parental WT Ct strain showed a modest reduction in inclusion formation (approximately 26% and 12% respectively) (Figure 5E). These results suggest that Cdu1 likely does not play a role in protecting Ct from IFNγ-mediated cellular immunity.

We also tested whether RNF213 localizes to inclusions that lack Cdu1, as observed in IFNγ-primed A549 cells infected with *garD:*:GII strains (Walsh et al., 2022). RNF213 did not localize to Ct inclusions when cells were infected with either WT Ct or *cdu1*::GII strains, regardless of whether or not the A549 cells were treated with IFNγ (Figures 5F and 5G). In contrast, RNF213 localized to approximately 37% of inclusions in cells infected with *garD*::GII mutants of unprimed

354 A549 cells, and 81% in IFNγ treated cells (Figures 5F and 5G). Based on these results, we
355 conclude that Cdu1 does not play a role in protecting Ct from IFNγ-induced antimicrobial activity.
356
357 **Cdu1 is required for F-actin assembly and Golgi ministack repositioning around the Ct**
358 **inclusion, and for MYPT1 recruitment to Ct inclusions**
359 InaC is required for Ct to assemble F-actin scaffolds and to reposition Golgi mini stacks
360 around the periphery of the inclusion membrane (Kokes et al., 2015; Wesolowski et al., 2017;
361 Haines et al., 2021). Because Cdu1 regulates InaC levels, we predicted that *cdu1* mutants
362 would phenocopy *inaC* mutants. We quantified the number of inclusions surrounded by F-actin
363 cages at 40 hpi. In cells infected with WT L2 (parental strain of M407 (*inaC* null), Nguyen and
364 Valdivia., 2012; Kokes et al., 2015), approximately 25% of inclusions were surrounded by F-
365 actin, consistent with previous observations (Chin et al., 2012; Kokes et al., 2015) (Figures 6A
366 and 6B, and Supplemental Figure 7). The number of inclusions surrounded by F-actin
367 decreased to approximately 7% in cells infected with an *inaC* null strain (M407) and increased
368 to approximately 49% in HeLa cells infected with an *inaC* null strain (M407) complemented with
369 wild type InaC (Figures 6A and 6B, and Supplemental Figure 7). Cells infected with *cdu1*::GII
370 mutants transformed with an empty plasmid or expressing Cdu1^{C345A}-Flag (DUB- Act-) and
371 Cdu1^{K268E}-Flag (Act-) resulted in approximately 8%,13%, and 10% of of F-actin positive
372 inclusions respectively (Figures 6A and 6B, and Supplemental Figure 7). In contrast, cells
373 infected with *cdu1*::GII mutants expressing Cdu1-Flag and Cdu1^{I225A}-Flag (DUB-) led to a
374 marked increase in F-actin inclusions (approximately 52% and 46% respectively) (Figures 6A
375 and 6B, and Supplemental Figure 7). From these observations we conclude that the acetylase
376 activity of Cdu1 is required for Ct to promote assembly of F-actin around the Ct inclusion likely
377 through the stabilization of InaC.
378

We next quantified Golgi dispersal in infected HeLa cells at 24 hpi, a process that is also dependent on InaC (Kokes et al., 2015; Wesolowski et al., 2017). In Hela cells infected with an *inaC* null strain (M407) Golgi dispersal was limited to approximately 26% of the Ct inclusion perimeter. In contrast, cells infected with either its parental WT L2 or with an *inaC* null strain (M407) complemented with wild type InaC, the Golgi is dispersed around 45% of the inclusion perimeter (Figures 6C and 6D, and Supplmental Figure 8). Similarly, Golgi dispersal around inclusions during infection with WT L2 and in *cdu1*::GII mutants expressing wild type Cdu1-Flag or Cdu1^{I225A}-Flag (DUB-) was approximately 43%, 41%, and 43% respectively (Figures 6C and 6D, and Supplmental Figure 8). In HeLa cells infected with *cdu1*::GII and *cdu1*::GII strains expressing Cdu1^{C345A}-Flag (DUB- Act-), and Cdu1^{K268E}-Flag (Act-), Golgi repositioning was restricted to approximately 24%, 23%, and 23% of inclusion perimeters respectively (Figures 6C and 6D, and Supplemental Figure 8). These results confirm that both InaC and Cdu1 are required for efficient repositioning of the Golgi around the Ct inclusion as previously reported (Kokes et al., 2015; Wesolowski et al., 2017; Pruneda et al., 2018; Auer et al., 2020) and that this process is independent of Cdu1's DUB activity but requires its acetylase activity. Moreover, our results suggest that Cdu1 promotes Golgi repositioning by protecting InaC-mediated redistribution of the Golgi around the Ct inclusion.

CTL0480 promotes recruitment of the myosin phosphatase subunit MYPT1 to the inclusion membrane where it regulates the extrusion of intact inclusions from host cells (Lutter et al., 2013; Shaw et al., 2018). Consistent with the gradual loss of CTL0480 from inclusions in cells infected with the *cdu1*::GII strain starting at 36 hpi (Figures 3E and Supplemental Figure 5) we also observed a complete loss of MYPT1 recruitment to inclusions by 48 hpi (Figures 6E and 6F).

Cdu1, InaC, IpaM, and CTL0480 are required for optimal extrusion of Ct from host cells

In the absence of Cdu1, the levels of InaC, CTL0480, and IpaM decreased late in infection (36 hpi and 48 hpi, Figures 3 and 4) suggesting that a prominent role of Cdu1 is to protect these Incs from degradation late in infection. At the end of its developmental cycle, *Chlamydia* exits host cells by promoting cellular lysis or by extrusion of intact inclusions (Hybiske and Stephens., 2007). Ct host cell exit by extrusion is an active process requiring a remodeling of the actin cytoskeleton and the function of Inc proteins (Hybiske and Stephens., 2007; Chin et al., 2012; Lutter et al., 2013; Shaw et al., 2018; Nguyen et al., 2018). CTL0480 recruits MYPT1 (an inhibitor of Myosin II motor complexes) to the inclusion membrane which prevents premature extrusion of Ct inclusions and loss of CTL0480 leads to increased rates of extrusion by Ct from infected HeLa cells (Lutter et al., 2013; Shaw et al., 2018) (Figure 7). Actin polymerization is also required for Ct extrusion (Hybiske and Stephens., 2007; Chin et al., 2012) suggesting that InaC dependent recruitment of F-actin to the inclusion may also contribute to optimal Ct extrusion. IpaM localizes to microdomains in the inclusion membrane that are proposed to function as foci for extrusion (Nguyen et al., 2018). Based on these observations, we postulated that Cdu1-mediated protection of CTL0480, InaC, and IpaM regulates the extrusion of Ct inclusions. We quantified the number of extrusions released from infected HeLa cells at 52 hpi and observed a 60% reduction in the number of extrusions in HeLa cells infected with the *cdu1*::GII strain relative to cells infected with WT L2 (Figures 7A and 7B). Complementation of *cdu1*::GII with either wild type Cdu1-Flag or Cdu1^{I225A}-Flag (DUB-) restored extrusion production to near wild type levels. In contrast, HeLa cells infected with *cdu1*::GII mutants expressing Cdu1^{K268E}-Flag (Act-), or *inaC* (*inaC*::GII, Wesolowski et al., 2017) and *ipaM* (*ipaM*::GII, Meier et al., 2020) null strains led to a 42%, 75%, and 58% reduction in extrusion production respectively (Figures 7A and 7B). The decrease in the number of extruded inclusions by these strains was not attributed to defects in inclusion biogenesis as they produced a

comparable number of inclusions at 48 hpi relative to cells infected with WT L2 (Supplemental Figure 9). Consequently, we infer that InaC, IpaM, and Cdu1 collectively contribute to the promotion of optimal extrusion of Ct inclusions from host cells, with Cdu1 playing a central regulatory role by protecting these effectors from degradation.

In contrast, infection of HeLa cells with a *ctl0480::GII* mutant strain led to an increase in the number of extruded inclusions as previously observed (Shaw et al., 2018) (Figures 7A and 7B). Therefore, even though the Cdu1-mediated protection of InaC and IpaM is important for the extrusion of inclusions and *cdu1* mutants phenocopy the loss of InaC and IpaM, the phenotypic similarities do not extend to the increased number of extruded inclusions observed in cells infected with the *ctl0480*::GII mutant strain (Figures 7A and 7B). We infer from these observations that functions for both InaC and IpaM in the extrusion of inclusions are epistatic to CTL0480. Extruded inclusions produced during infection of HeLa cells also varied in size with an average diameter of 40 μm (Figures 7A and 7C). Interestingly, the loss of IpaM and over expression of Cdu1-Flag and Cdu1^{I225A}-Flag (DUB-) shifted the size distribution of extrusions toward larger extrusions (Figures 7A and 7C) suggesting that Ct regulates the size of extruded inclusions through Cdu1.

Discussion

Several *Chlamydia* Inc proteins regulate interactions between the pathogenic vacuole and the host cytoskeleton, organelles, and vesicular trafficking pathways. These Inc proteins also modulate host cell death programs and promote *Chlamydia* exit from host cells (reviewed in Bugalhão and Mota., 2019)**.** Given the central roles that Incs play in promoting *Chlamydia* intracellular infection, it is not surprising that they are targeted for inactivation by host cellular defenses. In response, *Chlamydia* has evolved mechanisms to protect Incs. In this study we

show that the acetylase activity of the effector Cdu1 protects itself and three Inc proteins; InaC, IpaM, and CTL0480, from ubiquitination and degradation (Figure 8). Interestingly, all three Inc proteins play prominent roles in regulating the extrusion of inclusions from host cells (Figure 7). Observations that the encapsulation of *Chlamydia* within an extruded inclusion enhances survival of *Chlamydia* within macrophages (Zuck et al., 2017) together with the broad conservation of extrusion as an exit strategy among *Chlamydia* (Zuck et al., 2016) suggests that this mechanism is important for *Chlamydia* pathogenesis. Notably, a *cdu1* mutant strain (*cdu1*::Tn, Fischer et al., 2017) displays reduced bacterial loads in a murine model of upper genital tract infections (Fischer et al., 2017). While neither this strain nor our *cdu1*::GII mutant strain shows evident growth impairments during infection of Hela cells (data not shown), the observed reduction in bacterial load in the absence of Cdu1 in animal models of infection could potentially stem from defects in extrusion production or from perturbations in Cdu1-dependent regulation of extrusion size. Thus, targeting Inc proteins that regulate extrusion for Ub-mediated destruction may be advantageous for the host. For instance, targeting InaC for degradation would limit F-actin dependent extrusions (Hybiske and Stephens., 2013; Chin et al., 2012) and InaC-dependent microtubule scaffolds around the inclusion (Wesolowski et al., 2017; Haines et al., 2021). CTL0480 functions as an inhibitor of extrusions through its role in modulating the activity of myosin light chain 2 (MLC_2) (Lutter et al., 2013; Shaw et al., 2018). IpaM localizes to specialized microdomains in the inclusion membrane which are also sites of enrichment for over 9 inclusion membrane proteins including Ctl0480 and MrcA, both of which are required for *Chlamydia* extrusion (Mital et al., 2010; Lutter et al., 2013; Nguyen et al., 2018). We also find that the loss of IpaM shifted the size distribution of extrusions towards larger inclusions (Figure 7). We speculate that heterogeneity in the size of extrusions might facilitate uptake of some extrusions by innate immune cells at infected mucosal sites to promote *Chlamydia* LGV dissemination to distal sites in the genital tract and avoid clearance of *Chlamydia* by other immune cells (Zuck et al., 2017).

Effectors that modulate the activity of other translocated effectors are referred to as "metaeffectors", a term coined by Kubori and colleagues after observing that the *L. pneumophila* effector LubX which functions as an E3 ligase, ubiquitinates the translocated effector SidH leading to its degradation (Kubori et al., 2010). Several other effector-metaeffector interactions have been described in *L. pneumophila*, *Salmonella enterica*, and *Brucella abortus* which regulate the activity of other effectors either directly or indirectly by modifying the same host target or cellular process (Kubori et al., 2010; Neunuebel et al., 2011; Jeong et al., 2015; Urbanus et al., 2016; Smith et al., 2020; Iyer and Das., 2021). In this context we propose that Cdu1 functions as a metaeffector in Ct to protect multiple effectors. We also observed that Cdu1 interactions with InaC, IpaM, and CTL0480 likely occur independently from each other and that the kinetics of degradation in the absence of Cdu1 varies for each Inc (Figure 3).

Our findings indicate that the DUB activity of Cdu1 was not required to protect InaC, IpaM, and CTL0480 from ubiquitination. Instead we find that Cdu1's lysine acetylase activity is required to protect these Inc proteins and Cdu1 itself from ubiquitination. Indeed, we found that all three Incs and Cdu1 are acetylated at lysines in infected cells. However, we were unable to determine if lysine acetylation in all four proteins was dependent on Cdu1s' Act activity or if these PTMs are protective. Why the DUB activity of Cdu1 is unable to compensate for loss of its Act activity remains unknown. It is possible that Cdu1, like other DUBs, is regulated by PTMs (Komander et al., 2009a). For instance, phosphorylation of human CYLD inhibits its DUB activity towards TRAF2 while phosphorylation of human USP8 inhibits its DUB activity toward EGFR (Reiley et al., 2005; Mizuno et al., 2007). Mass spectrometry analysis of immunoprecipitated Flag tagged Cdu1 expressed in Ct revealed that Cdu1 is phosphorylated at multiple serine and threonine residues (Figure 4H) as previously suggested (Zadora et al., 2019). We identified three

PX(S/T)P MAPK phosphorylation consensus sequence motifs in the proline rich domain (PRD) of Cdu1, suggesting that MAPKs may regulate the DUB activity of Cdu1.

Cdu1 homologs are found in multiple *Chlamydia* species including *C. trachomatis*, *C. muridarum*, *C. suis*, *C. psitacci*, *C. abortus*, *C. caviae*, and *C. felis* but is notably absent in the genomes of *C. pneumoniae* and *C. pecorum*. The acquisition of a second deubiquitinase paralog (Cdu2) has also occurred in *C. trachomatis*, *C. muridarum*, and *C. suis*. In the genomes of all three species, *cdu2* resides directly adjacent to *cdu1*; an arrangement that presumptively arose from a gene duplication event. Cdu2 is a dedicated ULP with deubiquitinating and deneddylating activities (Misaghi et al., 2006; Pruneda et al., 2016). New evidence suggest that both paralogues might not be functionally redundant. The crystal structure of Cdu2 has revealed differences in residues involved in substrate recognition between Cdu1 and Cdu2 and that each paralog might recognize polyUb chains differently (Hausman et al., 2020). The processivity rates for removal of terminal Ub from polyUb chains also differs between both isopeptidases with Cdu2 exhibiting limited trimming of polyUb as compared to Cdu1 (Hausman et al., 2020). Moreover, Cdu2 lacks the proline rich domain found in Cdu1 which might be important for regulation of Cdu1 enzymatic activity. The presence of Cdu2 might also explain the low incidence of human and Ct proteins that were differentially ubiquitinated in the absence of Cdu1 (Figure 1). Whereas several *Chlamydia* species have acquired either one or two deubiquitinase paralogs, both *C. pneumoniae* and *C. pecorum* have not. Instead, both species have acquired an unrelated deubiquitinase (*Chla*OTU) belonging to the OTU family of proteases (Makarova et al., 2000; Furtado et al., 2013). Curiously, *Chla*OTU is also found in *C. psitacci*, *C. abortus*, *C. caviae*, and *C. felis* all of which encode only Cdu1 and is absent in *C. trachomatis*, *C. muridarum*, and *C. suis*, all of which encode Cdu1 and Cdu2. It is noteworthy that *Chlamydi*a species have independently acquired deubiquitinases multiple times (Cdu1, Cdu2, *Chla*OTU)

and that some of these deubiquitinases have evolved into moonlighting enzymes reflecting the diverse strategies adopted by pathogenic *Chlamydia* as they adapt to their particular niche.

Acknowledgements

We thank LifeSensors and the Duke Proteomics and Metabolomics Shared Resource Center for their proteomics services. We thank the Duke Light Microscopy Core Facility for microscopy services. We also thank Marcela Kokes for generating the IncA-Flag constructs used in this study. This work was supported by NIH grants GM142486 to J.N.P, AI103197 to J.C, AI140019 to R.J.B and AI134891 to R.H.V.

Author contributions

R.J.B and R.H.V designed the study. R.J.B wrote the manuscript with input from all listed authors. L.D generated the *cdu1*::GII strain. M.K verified generation of the *cdu1*::GII mutant strain and showed interaction of Cdu1-GFP variants with InaC, IpaM, and CTL0480 in transfected HEK cells. R.K.D and S.C.W contributed equally to this work and quantified inclusion production and RNF213 localization in unprimed and IFNγ-primed A549 cells. R.J.B performed all other experiments. J.C, B.S.S, and J.N.P shared reagents. R.J.B and R.H.V proofed the manuscript.

Declaration of interests

R.H.V is a founder of Bloom Sciences (San Diego, CA), which is a microbiome therapeutics company. Findings reported in this study are unrelated to the work being performed with Bloom Sciences.

Material and Methods

Key Resource Table

REAGENT or RESOURCE	SOURCE	IDENTIFIER
Antibodies		
See S. Table 9		
Bacterial and virus strains		
Chlamydia trachomatis LGV biovar L2 434 Bu (L2)	Richard Stephens (UC Berkeley)	N/A
L2 pBOMB-MCl (Parent: LGV L2 434 Bu)	This paper	N/A
L2 pBOMB-MCl_CTL0480-3XFlag (Parent: LGV L2 434 Bu)	This paper	N/A
L2 pBOMB-MCl_IpaM-3XFlag (Parent: LGV L2 434 Bu)	This paper	N/A
L2 pBOMB-MCl_Cdu1-3XFlag (Parent: LGV L2 434 Bu)	This paper	N/A
L2 pBOMB-MCl_Cdu1 ^{C345A}-3XFlag (Parent: LGV L2 434 Bu)	This paper	N/A
L2 pBOMB-MCl_Cdu1 ^{K268E}-3XFlag (Parent: LGV L2 434 Bu)	This paper	N/A
L2 *cdu1*::GII *aadA* (Parent: LGV L2 434 Bu)	This paper	N/A
L2 *cdu1*::GII *aadA* pBOMB-MCl (Parent: L2 *cdu1*::GII *aadA*)	This paper	N/A
L2 *cdu1*::GII *aadA* pBOMB-MCl_Cdu1-3XFlag (Parent: L2 *cdu1*::GII *aadA*)	This paper	N/A
L2 *cdu1*::GII *aadA* pBOMB-MCl_Cdu1 ^{C345A}-3XFlag (Parent: L2 *cdu1*::GII *aadA*)	This paper	N/A
L2 *cdu1*::GII *aadA* pBOMB-MCl_Cdu1 ^{I225A}-3XFlag (Parent: L2 *cdu1*::GII *aadA*)	This paper	N/A
L2 *cdu1*::GII *aadA* pBOMB-MCl_Cdu1 ^{K268E}-3XFlag (Parent: L2 *cdu1*::GII *aadA*)	This paper	N/A
L2 Rif-R (Parent: L2 434 Bu)	Nguyen et al., 2012	N/A
M407 (*inaC C307T*, InaC Q103*) (Parent: L2 Rif-R)	Kokes et al., 2015	N/A
M407 p2TK2 (Parent: M407)	Kokes et al., 2015	N/A
M407 p2TK2_InaC (Parent: M407)	Kokes et al., 2015	N/A
M407 p2TK2_InaC-3X Flag (Parent: M407)	This paper	N/A
inaC::GII *bla* (Parent: L2 434 Bu)	Wesolowski et al., 2017	N/A
ipaM::GII *cat* (Parent: L2 434 Bu)	Meier et al., 2022	N/A
ctl0480::GII *aadA* (Parent: L2 434 Bu)	Shaw et al., 2018	N/A
M923 (*incA C589T*, IncA R197*) (Parent: L2 Rif-R)	Kokes et al., 2015	N/A
M923 pBOMB-MCl (Parent: L2 M923)	Sixt et al., 2017	N/A
L2 434 Bu (Parent of L2 *garD*::GII)	Walsh et al., 2022	N/A

L2 *ctl0390*::GII *aadA* (*garD*::GII)	Walsh et al., 2022	N/A
Biological samples		
N/A		
Chemicals, peptides, and recombinant proteins		
PR-619 (DUB inhibitor)	Sigma-Aldrich	Cat# SML0430
MG132 (proteasome inhibitor)	Sigma-Aldrich	Cat# 474791
TUBE-1 (pUb affinity capture reagent)	LifeSensors	Cat# UM401M
Acti-stain™ 488 (Phalloidin 488)	Cytoskeleton Inc.	Cat# PHDG1
ChromoTek GFP-Trap® Agarose	Proteintech	Cat# gta
Protein A/G PLUS-Agarose	Santa Cruz Biotechnology	Cat# sc-2203
3xFLAG peptide	APExBIO	Cat# A6001
Recombinant human interferon gamma (IFNγ)	Millipore	Cat# IF005
LGV L2 434 Bu Cdu1 recombinant protein	Jonathan Pruneda (Oregon Health and Science University)	N/A
Critical commercial assays		
TargeTron™ gene knockout system	Sigma-Aldrich	Cat# TA0100
Deposited data		
C. trachomatis LGV L2 434 Bu proteome	NCBI	NCBI:txid47472
Homo sapiens (Human) proteome	UniProt	Proteome ID: UP000005640
TUBE-1 affinity capture proteomics data	LifeSensors	Supplemental Table 1
Experimental models: Cell lines		
Hela cells	ATCC	Cat# CCL-2 RRID:CVCL_0030
Vero cells	ATCC	Cat# CCL-81 RRID:CVCL_0059
HEK 293T cells	ATCC	Cat# CRL-3216 RRID:CVCL_0063
A549 cells	ATCC	Cat# CCL-185 RRID:CVCL_0023
Experimental models: Organisms/strains		
Chlamydia trachomatis LGV L2 434 Bu	Richard Stephens (UC Berkeley)	N/A
Oligonucleotides		
See S. Table 10		
Recombinant DNA		
Plasmid: pDFTT3-aadA_Cdu1 635/636	This paper	N/A
Plasmid: pOPIN-GFP_Cdu1 FL (aa 1-401)	Jonathan Pruneda (Oregon Health and Science University)	N/A
Plasmid: pOPIN-GFP_Cdu1 TMD- (aa 71-401)	Jonathan Pruneda (Oregon Health and Science University)	N/A
Plasmid: pOPIN-GFP_Cdu1 CD- (aa 1-130)	Jonathan Pruneda (Oregon Health and Science University)	N/A

Plasmid: pCDNA-DEST53 (w/o GFP)_InaC (CT813)-3XFLAG	This paper	N/A
Plasmid: pcDNA3.1/nV5-DEST_IpaM	This paper	N/A
Plasmid: pcDNA3.1/nV5-DEST_CTL0480 p	This paper	N/A
Plasmid: pcDNA3.1/nV5-DEST_CpoS	This paper	N/A
Plasmid: pBOMB4-MCI_CTL0480-3X Flag	This paper	N/A
Plasmid: pBOMB4-MCI_IpaM-3X Flag	This paper	N/A
Plasmid: pBOMB4-MCI_Cdu1-3XFlag	This paper	N/A
Plasmid: pBOMB4-MCI_Cdu1 C345A-3XFlag	This paper	N/A
Plasmid: pBOMB4-MCI_Cdu1 I225A-3XFlag	This paper	N/A
Plasmid: pBOMB4-MCI_Cdu1 K263E-3XFlag	This paper	N/A
Plasmid: p2TK2_SW2_InaC-3XFlag	This paper	N/A
Software and algorithms		
Targetronics	Targetronics, LLC	www.targetrons.com
Proteome Discoverer 2.3	Thermo Fisher Scientific	https://www.thermofisher.com/us/en/home/industrial/mass-spectrometry/liquid-chromatography-mass-spectrometry-lc-ms/lc-ms-software/multi-omics-data-analysis/proteome-discoverer-software.html
Mascot software	Matrix Science	https://www.matrixscience.com
MaxQuant 1.6.2.3		https://www.maxquant.org
Scaffold PTM	Proteome Software	https://www.proteomesoftware.com/products/scaffold-ptm
VolcaNoseR	Goedhart, and Luijsterburg., 2020	https://huygens.science.uva.nl/VolcaNoseR/
Metascape	Zhou et al., 2019	https://metascape.org/gp/index.html#/main/step1
DAVID Bioinformatic Resources	Huang et al., 2009a., Huang et al., 2009b	https://david.ncifcrf.gov/tools.jsp
Image J	Schneider et al., 2012	https://imagej.nih.gov/ij/
NEBaseChanger	New England Biolabs	https://nebasechanger.neb.com
Prism 9	GraphPad	https://www.graphpad.com/updates/prism-900-release-notes
HCS Studio Cell Analysis Software	Thermo Fischer Scientific	Cat# CX51110
Other		
N/A		

Resource Availability

Materials availability

- All newly generated materials associated with this study will be freely available upon request.

Data and code availability

- Unprocessed (raw) proteomics data received from LifeSensors can be found in Supplemental Table 1.

- Original data used for microscopy and western blots in this study can be found at Mendeley data repository (data.mendeley.com):

Bastidas, Robert; Kędzior, Mateusz; Davidson, Robert; Walsh, Stephen; Dolat, Lee; Sixt, Barbara; Pruneda, Jonathan; Coers, Jörn; Valdivia, Raphael (2023), "The acetylase activity of Cdu1 regulates bacterial exit from infected cells by protecting *Chlamydia* effectors from degradation", Mendeley Data, V1, doi: 10.17632/xt3nmkm375.1

- Any additional information required to reanalyze the data reported in this paper is available upon request.

- This paper does not report original code.

Experimental Model And Subject Details

Cell lines

Vero (CCL-81; RRID:CVCL_0030), HeLa (CCL-2; RRID:CVCL_0059), HEK293T (CRL-3216; RRID:CVCL_0063), and A549 (CCL-185; RRID:CVCL_0023) cells were purchased from ATCC and cultured in High Glucose Dulbecco's Modified Eagle's Medium supplemented with L-glutamine, sodium pyruvate (DMEM; Gibco) and 10% fetal bovine serum (FBS; Sigma-Aldrich). Cells were grown at 37°C in a 5% CO2 humidified incubator. Vero, Hela, and HEK293T cells were derived from females while A549 cells were derived from a male. All four cell lines have been authenticated by the Duke Cell Culture and DNA analysis facility.

Chlamydia strains and propagation

Chlamydia strains used in this study are listed in the Key Resources Table. Ct strains were propagated in Vero cells and harvested by osmotic lysis at 48 hours post infection. Following lysis extracts were sonicated and bacteria pelleted by centrifugation at 21,000 x g. Bacteria were resuspended in SPG storage buffer (75g/L sucrose, 0.5 g/L KH_4HPO_4, 1.2 g/L Na_2HPO_4, 0.72 g/L glutamic acid, pH 7.5) and stored as single use aliquots at -80°C.

Method Details

Chlamydia infections

Chlamydia infections were synchronized by centrifugation (2,500 x *g* for 30 minutes at 10°C) onto HeLa cell monolayers and incubated for the indicated times. Co-infections were performed by infecting HeLa cell monolayers at a 1:1 ratio using MOIs of 2 for each co-infecting strain.

Insertional mutagenesis of CTL0247 (*cdu1*)

Primer sequences for TargeTron™ mediated mutagenesis of the LGV L2 434 Bu *cdu1* (CTL0247) ORF were designed at the TARGETRONICS, LLC web portal (www.targetrons.com). IBS1/2, EBS1/delta, and EBS2 primers (primer sequences are listed in

S. Table 10) were used in a PCR reaction to generate homing sequences for TargeTron™ integration between nucleotides 635 and 636 of the *cdu1* ORF using a TargeTron™ gene knockout system (Sigma-Aldrich; TA0100) according to the manufacturer instructions. Homing sequences were gel purified, digested with HindIII and BsrGI, and ligated into HindIII and BsrGI digested pDFTT3-*aadA* (Lowden et al., 2015). Ligations were transformed into *E. coli* DH5α, clones isolated, and *cdu1* redirected pDFTT3-aadA plasmids identified by restriction digest and verified by Sanger sequencing (Eton Bioscience) using a T7-promoter specific primer. The resulting plasmid was transformed into a *C. trachomatis* LGV L2 434 Bu strain and transformants selected with 150 μg/mL spectinomycin and plaque purified as previously described (Kędzior and Bastidas., 2019). Insertion of the GII *aadA* intron at the *cdu1* locus was verified by PCR analysis (S. Figure1) using primers that amplify amplicons spanning the *cdu1*::GII 5' (RBP409 and RBP436) and 3' (RBP468 and RBP118) junctions, the *cdu1* CDS (RBP409 and RBP118), and the *aadA* CDS (RBP512 and RBP513). Primer sequences are listed in S. Table 10. Loss of Cdu1 protein was verified by western blot and indirect immunofluorescence analysis (S. Figures 2A and 2B).

Analysis of *cdu1* and *cdu2* transcription by RT-PCR

Confluent HeLa cell monolayers (2.9 x 10^6 cells/infection) were infected with wild type L2 434 Bu or L2 *cdu1*::GII *aadA* strains. At 24 hpi, total RNA was isolated with a Qiagen RNeasy kit (Qiagen; 74004) according to the manufacturer instructions. Total RNA was treated twice with DNAse I (NEB; M0303S) and used for cDNA synthesis using a SuperScript IV Reverse Transcriptase kit (Thermo Fisher Scientific; 18090010). cDNAs synthesized with and without reverse transcriptase were used as templates for PCR analysis (S. Figure 2C) using primers that amplify amplicons spanning the *cdu*1 (CTL0247_F and CTL0247_R) and *cdu2* ORFs

(CTL0246_F and CTL0247_R), and the intergenic junction between the *cdu1* and *cdu2* ORFs (CTL0246-0247_F and CTL0246-0247_R). Primer sequences can be found in the S. Table 10.

TUBE1 based global ubiquitin profiling

Confluent HeLa cell monolayers (5.04 x 10^6 cells/infection) were mock infected or separately infected with WT LGV L2 434 Bu or a L2 *cdu1*::GII *aadA* strain at MOIs of 3. At 24 hpi cells were collected and spun down (700 x *g* for 10 minutes), frozen at -80°C and shipped on dry ice to LifeSensors (Malvern, PA) for quantitative TUBE1-based Mass Spectrometry Analysis. Cell pellets from three independent biological replicates were sent to LifeSensors for analysis. Cell were subsequently lysed in lysis buffer (50 mM Tris-HCL, pH 7.5, 150 mM NaCl, 2 mM EDTA, 1% NP-40, 10% glycerol, 1% Sodium Deoxycholate) supplemented with a protease inhibitor cocktail, the DUB inhibitor PR-619 (Sigma-Aldrich; SML0430), and the proteasomal inhibitor MG-132 (Sigma-Aldrich; 474791). Lysates were clarified by high-speed centrifugation (14,000 x *g*, 10 minutes, 4°C) and supernatants containing 5 mg of protein were equilibrated with magnetic TUBE-1 (LifeSensors; UM401M) and incubated overnight at 4°C under rotation. TUBEs were isolated with a magnetic stand and washed sequentially with PBST and TUBE wash buffer. Poly-ubiquitinated and associated proteins were eluted with TUBE elution buffer. Eluted supernatants were neutralized with neutralization buffer and loaded onto SDS-gels and run until SDS buffer reached 0.5 cm into the gel. Gels were stained with Coomassie Blue and lanes excised, reduced with TCEP, alkylated with iodoacetamide, and digested with Trypsin (Trypsin Gold, Mass Spectrometry Grade) (Promega; V5280). Tryptic digests were analyzed using a 150 min LC run on a Thermo Scientific™ Q Exactive HF Orbitrap™ LC-MS/MS system. MS data was searched against the UniProt human database (UniProt; Proteome ID: UP000005640) and the *Chlamydia trachomatis* L2 434 Bu reference database (NCBI:txid47472) using MaxQuant 1.6.2.3 (https://www.maxquant.org). Proteins, peptides, and site identification

was set to a false discovery rate of 1%. N-terminal acetylation, Met oxidation, and diGly remnant on lysine residues was also identified. All peptides and proteins identified can be found in S. Table 1. The intensities (sum of all peptide MS peak areas for a protein or ubiquitinated peptide) for each protein and ubiquitinated peptide across all three biological replicates were used to determine mean intensities and to calculate *p*-values based on one-way student t-tests. Volcano plots of mean intensities vs. *p*-values were generated with VolcaNoseR (Goedhart and Lujsterburg., 2020) (https://huygens.science.uva.nl/VolcaNoseR/) and used to identify significantly enriched proteins and ubiquitinated peptides. Data used to generate each Volcano plot can be found in S. Table 2. Pathway enrichment analysis was performed with Metascape (Zhou et al., 2019) (https://metascape.org/gp/index.html#/main/step1) and DAVID bioinformatic resources (Huang et al., 2009a; Huang et al., 2009b) (https://david.ncifcrf.gov/tools.jsp).

Inhibitors, antibodies, western blots, and densitometry analysis

MG-132 (25 μM) (Sigma-Aldrich; 474791) was added to infected cell monolayers 5 hours prior to extract preparations. Recombinant Cdu1 protein (LGV L2 434 Bu, amino acids 71-401) was generated as previously described (Pruneda et al., 2018) and kindly provided by Jonathan Pruneda (Oregon Health and Science University, OR). Recombinant Cdu1 protein was used to generate antibodies in immunized New Zealand White rabbits. Cdu1 antisera was pre-adsorbed with crude cell extracts from HeLa cells infected with a *cdu1*::GII *aadA* strain. Pre-adsorbed antisera was used for western blot analysis at a 1:500 dilution in a solution containing 5% BSA supplemented with crude extracts from HeLa cells infected with a *cdu1*::GII *aadA* strain (0.1mg/mL total protein). Antibodies, antibody dilutions, and antibody diluents used in this study are listed in S. Table 9. For western blot analysis, lysates from infected HeLa cell monolayers (2.4×10^6 cells) were prepared by incubating cell monolayers with boiling hot 1% SDS lysis buffer (1% SDS, 100 mM NaCl, 50 mM Tris, pH 7.5). Lysates were collected, briefly sonicated, and total protein concentration measured with a DC™ Protein Assay Kit (BIO-RAD; 5000111). 8

μg (Slc1 and alpha Tubulin blots) and 25 μg of total protein lysates (all other blots) were loaded onto 4-15% Mini-PROTEAN and TGX Stain Free™ Protein Gels (BIO-RAD; 4568084), transferred to PVDF membranes (BIO-RAD; 1620177), blocked with 5% Milk/TBSt, and incubated with primary antibodies overnight at 4°C. Protein signals were detected with Goat anti mouse (H+L) IgG (ThermoFisher scientific; 31430) or Goat anti rabbit (H+L) IgG HRP (ThermoFisher scientific; 31460) conjugated secondary antibodies (1:1000 in 5% Milk/TBSt) and SuperSignal West Femto HRP substrate (ThermoFisher scientific; 34096). Antibody bound membranes were imaged with a LI-COR Odyssey Fc Imager (LI-COR, Inc.). Varying amounts of protein extracts were used to determine the linear range of detection for InaC, IpaM, and Slc1 antibodies prior to quantification of western blot images (data not shown). Protein bands were quantified using western blot densitometry analysis with LI-COR Image Studio Software (LI-COR, Inc.). InaC and IpaM densitometry measurments were normalized to corresponding Slc1 densitometry measurments.

Immunofluorescence microscopy

HeLa cells were grown on coverslips to 50% confluency (0.1 x 10^5 cells) and infected at MOIs of 0.6. At indicated times, infected cells were separately fixed with ice cold Methanol or with warm PBS containing 4% formaldehyde for 20 minutes. After fixative removal, cells were washed with PBS and formaldehyde fixed cells were incubated either in 5% BSA/PBS supplemented with 0.1% Triton X-100 or in 5% BSA/PBS supplemented with 0.05% Saponin for 30 minutes with gentle rocking. Following washing with PBS, Methanol fixed cells were incubated with primary antibodies diluted in 5% BSA/PBS and formaldehyde fixed cells were incubated with primary antibodies diluted in 5% BSA/PBS supplemented with 0.1% Triton X-100 or 0.05% Saponin for 1 hour with gentle rocking. Dilutions for each antibody used can be found in S. Table 9. Methanol fixed cells were washed with PBS and incubated with secondary antibodies diluted in

5% BSA/PBS and supplemented with Hoechst 33342 (2 µg/mL) (ThermoFisher Scientific; H3570). Formaldehyde fixed cells were washed and incubated with 5% BSA/PBS supplemented with 0.1% Triton X-100 and Hoechst or 0.05% Saponin and Hoechst for 1 hour protected from light and with gentle rocking. For detection of F-actin, Phalloidin conjugated to Alexa Fluor™ 488 (1:5000) (Act-Stain 488 Phalloidin; Cytoskeleton Inc.; PHDG1) was added for the last 20 minutes of incubation with the secondary antibodies. Coverslips were transferred to glass slides, mounted with 10 µL of Vectashield (Vector Labs; H-1000) and incubated over night at room temperature prior to imaging. Secondary antibodies used were goat anti-mouse (H+L) IgG (ThermoFisher scientific; A-11001 and A-21235) and goat anti-rabbit (H+L) IgG (ThermoFisher scientific; A-11008 and A-21244) conjugated to Alexa Fluor™ 488 and Alexa Fluor™ 647. All of the antibodies used for indirect immunofluorescence analysis were analyzed under all three staining conditions (Methanol, Formaldehyde/Triton X-100, and Formaldehyde/Saponin).

Quantitative immunofluorescent microscopy for RNF213 was performed as previously described (Walsh et. al., 2022). Briefly, A549 cells were grown on coverslips in 24-well plates to full confluency (~2 x 10^5 cells). Cells were infected with indicated *C. trachomatis* strains at an MOI of 2. At 3 hours post-infection, all cells were given fresh DMEM supplemented with L-tryptophan (100 µg/mL) with half of the wells given interferon-gamma (100U/mL; Millipore, IF005). At 24 hours post-infection, cells were fixed with cold, 4% PFA in PBS for 20 minutes. Cells were permeabilized with ice-cold methanol for 1 minute and blocked in PBS containing 5% BSA and 2.2% glycine for 30 minutes. Antibody incubations and microscope slide mounting was performed as described. Samples were blinded using tape and imaged on a Zeiss Axio Observer.Z1 epifluorescent microscope. For each sample, at least 6 separate fields of view and 100 *Chlamydia* inclusions were captured, saved and further blinded using the ImageJ Blind Analysis Tool plugin (https://imagej.net/plugins/blind-analysis-tools). Quantification of the

731 number of inclusions with RNF213 targeted to the inclusion membrane was performed using
732 ImageJ (Schneider et al., 2012). Targeted inclusions were scored as having the indicated
733 protein signal colocalize with >50% of the inclusion membrane signal (incA positive antibody
734 staining).
735
736 Representative images were acquired with an inverted confocal laser scanning microscope
737 (Zeiss 880) equipped with an Airyscan detector (Hamamatsu) and with diode (405 nm), argon
738 ion (488 nm), double solid-state (561 nm) and helium-neon (633) lasers. Images were acquired
739 with a 63x C-Apochromatic NA 1.2 oil-objective (Zeiss). Images acquired in Airyscan mode were
740 deconvoluted using automatic Airyscan processing in Zen software (Zeiss). Image acquisition
741 was performed at the Light Microscopy Core Facility at Duke University. Images used for
742 quantification were captured in an inverted microscope (Ti2-Nikon instruments) equipped with
743 an ORCA Flash 4.0 V3 sCMOS camera (Hamamatsu) and a SOLA solid-state white light
744 illuminator (Lumencro). Images were acquired using a 60x Plan Apochromatic NA 1.40 oil
745 objective. All images were opened with ImageJ (Schneider et al., 2012) and only linear
746 adjustments were made to fluorescence intensity for the entire image. Images were exported as
747 TIFFs and compiled with Adobe suite software (Illustrator).
748
749 **Vector construction and *C. trachomatis* transformation**
750 *Constructs used in co-transfection experiments:* Mammalian vectors expressing Cdu1-GFP
751 constructs were kindly provided by Jonathan Pruneda (Oregon Health and Science University,
752 OR). Briefly, geneblocks encoding full length Cdu1 (LGV L2 434 Bu, CTL0247) (amino acids 1-
753 401), Cdu1 lacking its transmembrane domain (amino acids 71-401), and Cdu1 lacking its
754 catalytic domain (amino acids 1-130) were generated and inserted into the pOPIN-GFP vector
755 (Berrow et al., 2007) by In-Fusion™ cloning (Takara Bio; 638947), resulting in Cdu1 constructs
756 with a C-terminal eGFP-His tag preceded by a 3C protease cleavage site. The Flag-InaC

mammalian expression vector was derived from a Gateway™ entry clone containing the *C. trachomatis* Serovar D/UW-3/CX CT813 (*inaC*) ORF (amino acids 41-264) obtained from a *C. trachomatis* ORFeome library (Roan et al., 2006). The entry vector was used as a donor plasmid for Gateway™ based transfer into a modified pcDNA™ DEST53 (ThermoFisher Scientific; 12288015) vector in which the cycle 3 *GFP* ORF was removed. A NEB Q5®-Site Directed Mutagenesis Kit (New England Biolabs; E0554S) was used to introduce a 3X Flag epitope tag at the N-terminus of the CT813 ORF and a stop codon at the end of the CT813 ORF. L2 *ipaM* (CTL0476), L2 CTL0480, and L2 *cpoS* (CTL0481) ORFs were PCR amplified from cell lysates derived from Vero cells infected with wild type L2 LGV 434 Bu with primers containing attB sequences (primers *ipaM* forward, *ipaM* reverse, CTL0480 forward, CTL0480 reverse, *cpoS* forward, and *cpoS* reverse). Primer sequences can be found in the S. Table 10. PCR amplicons were used as donors for Gateway™ BP Clonase™ based transfers into the donor vector pDONR™221 (ThermoFisher Scientific; 12536017) to generate entry plasmids. Entry plasmids were used to transfer *ipaM*, CTL0480, and *cpoS* into the Gateway™ destination vector pcDNA™3.1/nV5-DEST (ThermoFisher Scientific; 12290010) by Gateway™ LR Clonase™ based reactions. The resulting mammalian expression vectors express IpaM, CTL0480, and CpoS with V5-epitopes fused to their N-terminus.

pBOMB4-MCI based plasmids. CTL0480 and *ipaM* ORFs were amplified by PCR from cell extracts derived from Vero cells infected with wild type LGV L2 434 Bu. The CTL0480 ORF, 149 b.p of upstream sequence, and a 3X FLAG epitope was amplified by PCR using primers RBP628 and RBP629. The CTL0476 (*ipaM*) ORF, 400 b.p of upstream sequence, and a 3X FLAG epitope was amplified with primers RBP623 and RBP624. CTL0480 and *ipaM* amplicons were digested with Not1 and Pst1 and cloned into Not1 and Pst1 digested pBOMB4-MCI (Bauler and Hackstadt., 2014) to generate pBOMB4-MCI_CTL0480-3X Flag and pBOMB4-MCI_IpaM-3X Flag plasmids respectively. pBOMB4-MCI_Cdu1-3XFlag plasmids were

generated by PCR amplification of 175 b.p of genomic sequence directly upstream of the L2 434 Bu CTL0247 (*cdu1*) ORF and the entire *cdu1* ORF tagged with a C-terminal 3X Flag epitope tag (primers RBP460 and RBP461). PCR amplicons were generated from gradient purified LGV L2 434 Bu EBs and cloned into a pCR™-Blunt II TOPO® vector using a Zero Blunt™ TOPO™ PCR cloning Kit (ThermoFisher Scientific; K2800J10) according to the manufacturer instructions. Cdu1 catalytic variants were generated with a NEB Q5®-Site Directed Mutagenesis Kit (New England Biolabs; E0554S) using the *cdu1*p-*cdu1*-3X Flag construct cloned into pCR™-Blunt II TOPO® as a template and following the manufacturer instructions. Primers for introducing base pair changes were designed on the NEBaseChanger website (https://nebasechanger.neb.com). The Cdu1^{C345A} variant was generated by changing the *TGC* codon located at positions 1033-1035 in the *cdu1* ORF to *GCT* (primers RBP525 and RBP526). The Cdu1^{I225A} variant was generated by substituting the *ATC* codon located at positions 673-675 for *GCT* (primers RBP527and RBP528). The Cdu1^{K268E} variant was generated by introducing an *A802G* base pair substitution (primers RBP529 and RBP530). Wild type *cdu1*p-*cdu1*-3XFLAG and all three *cdu1* variants were digested with Not1 and Pst1 and ligated into Not1 and Pst1 digested pBOMB4-MCI (Bauler and Hackstadt., 2014). Primer sequences can be found in the S. Table 10.

p2TK2_SW2-inaC-3XFlag. The CTL0184 (*inaC*) ORF and 250 b.p of upstream sequence was amplified by PCR from cell extracts derived from Vero cells infected with L2 434 Bu and cloned into the p2TK2_SW2 vector (Agaisse and Derré., 2013). A NEB Q5®-Site Directed Mutagenesis Kit (New England Biolabs; E0554S) was used to insert a 3X FLAG epitope sequence at the C-terminus (stop codon removed) of the CTL0184 ORF to generate the p2TK2_SW2-InaC-3XFlag plasmid.

pBOMB4-MCI based plasmids and p2TK2_SW2-InaC-3X Flag plasmids were transformed into corresponding *Chlamydia* strains, and transformants were selected with 10 U/mL Penicillin G and plaque purified as previously described (Kędzior and Bastidas., 2019). All primer sequences and plasmids generated in this study are listed in S. Table 10 and Key Resources Table.

Subcellular fractionation

HeLa cells (2.16 x 10^7 cells/strain) seeded in six well plates were mock infected or infected with *Chlamydia* L2 434 Bu strains. At indicated time points cells were washed with ice-cold PBS, collected in ice-cold PBS with a cell scraper, and transferred to 15 mL conical tubes. Cell suspensions were centrifuged at 500 x g for 5 minutes at 4°C and cell pellets were resuspended in 400 µL of ice-cold subcellular fractionation buffer (20 mM HEPES (pH 7.4), 10 mM KCl, 2mM $MgCl_2$, 1mM EDTA, 1mM EGTA) supplemented with 1mM DTT and a 1x cOmplete Mini-EDTA free protease inhibitor cocktail (Sigma-Aldrich; 11836170001). Cells were incubated on ice for 20 minutes and lysed with 30 strokes of a Dounce homogenizer. Cell lysates were sequentially centrifuged twice at 720 x g for 5 minutes at 4°C to remove intact nuclei. Supernatants were centrifuged at 10,000 x g for 5 minutes at 4°C and the heavy membrane (inclusion) fraction was recovered and resuspended in IP lysis buffer (25 mM Tris-Hcl, 150 mM NaCl, 1% NP-40, 5% Glycerol) supplemented with 1mM PMSF and a 1x cOmplete Mini-EDTA free protease inhibitor cocktail (Sigma-Aldrich; 11836170001).

Immunoprecipitations (IPs)

Transfections and GFP-immunoprecipitations: HEK 293T cell monolayers (1.32 x 10^7 cells/transfection) seeded in 10 cm cell culture dishes pre coated with poly-L-Lysine (Sigma-Aldrich; P4707) were grown to 50% confluency and transfected with 10 µg of each plasmid used

per co-transfection in a 1.5 to 1 ratio of jetOPTIMUS® (Polyplus; 101000051) transfection reagent to total plasmid DNA according to the manufacturer instructions. At 24 hpi, transfected cells were lysed in IP lysis buffer (described above) supplemented with 1mM PMSF and 1x cOmplete Mini-EDTA free protease inhibitor cocktail (Sigma-Aldrich; 11836170001). Lysates were transferred to Eppendorf tubes, sonicated, and cleared by centrifugation (21,000 x *g*, 15 minutes, 4°C). Supernatants containing 2 mg of total protein were incubated with magnetic GFP-Trap® agarose (Proteintech; gta) for 1 hour at 4°C with rotation. Beads were washed according to manufacturer instructions and immunoprecipitated proteins eluted with 2X Laemmli sample buffer.

Flag immunoprecipitations: Mock and infected HeLa cell monolayers (1.44 x 10^7 cells) grown in six well plates were lysed in IP lysis buffer (described above) and transferred to Eppendorf tubes. Lysates were sonicated and cleared by centrifugation (21,000 x *g*, 15 minutes, 4°C). Supernatants containing 2 mg of total protein were pre-cleared by incubating with Protein A/G PLUS-Agarose (Santa Cruz Biotechnology; sc-2203) for 30 minutes at 4°C followed by sedimentation of agarose resins by centrifugation. Supernatants were incubated with M2-anti Flag mouse mAb (1:400) (Sigma-Aldrich; F1804) overnight at 4°C with rotation followed by incubation with Protein A/G PLUS-Agarose for 3 hours at 4°C with rotation. Agarose resins were sedimented and washed according to manufacturer instructions and immunoprecipitated proteins eluted with 50 µL of 100 µg/mL 3xFLAG peptides (APExBIO; A6001).

Acetylated lysine immunoprecipitations. Heavy membrane (inclusion) subcellular fractions isolated from infected HeLa cells and containing 1 mg of total protein were pre-cleared by incubating with Protein A/G PLUS-Agarose (Santa Cruz Biotechnology; sc-2203) for 30 minutes at 4°C followed by sedimentation of agarose resins by centrifugation. Supernatants were

incubated with an anti-acetylated lysine rabbit antibody (Cell signaling; #9441) (1:100) overnight at 4°C with rotation followed by incubation with Protein A/G PLUS-Agarose for 3 hours at 4°C with rotation. Agarose resins were sedimented and washed according to manufacturer instructions and immunoprecipitated proteins eluted with 50 µL of 2X Laemmli sample buffer.

Input (8 µg of total protein for Slc1 and alpha Tubulin blots, and 25 µg for all other blots) and immunoprecipitates (GFP, Flag, proteins acetylated at lysines) were loaded onto 4-15% Mini-PROTEAN and TGX Stain Free™ Protein Gels (BIO-RAD; 4568084), transferred to PVDF membranes (BIO-RAD; 1620177), blocked with 5% Milk/TBSt, and incubated with primary antibodies overnight at 4°C. Protein signals were detected with Goat anti mouse (H+L) IgG (ThermoFisher scientific; 31430) or Goat anti rabbit (H+L) IgG HRP (ThermoFisher scientific; 31460) conjugated secondary antibodies (1:1000 in 5% Milk/TBSt) and SuperSignal West Femto HRP substrate (ThermoFisher scientific; 34096). Antibody bound membranes were imaged with a LI-COR imaging system (LI-COR, Inc.).

Identification Cdu1 lysine acetylation and phosphorylation sites by LC-MS/MS

HeLa cell monolayers (8.64 x10^7 cells/strain) grown in six well plates were infected with a wild type L2 strain transformed with empty pBOMB4-MCI (Bauler and Hackstadt., 2014) plasmid or with a wild type L2 strain transformed with a pBOMB4-MCI_*cdu1*-3X Flag plasmid. At 24 hpi infected cells were lysed and Flag tagged Cdu1 was immunoprecipitated as described above. Flag eluates from 3 independent biological replicates were sent to the Proteomics and Metabolomics Shared Resource Facility at Duke University for quantitative LC-MS/MS analysis. Samples were spiked with undigested casein, reduced with 10 mM dithiothreitol, and alkylated with 20 mM iodoacetamide. Eluates were then supplemented with 1.2% phosphoric acid and S-Trap (Protifi) binding buffer (90% Methanol, 100 mM TEAB). Proteins were trapped on the S-

Trap, digested with 20 ng/µL Trypsin (Trypsin Gold, Mass Spectrometry Grade) (Promega; V5280), and eluted with 50 mM TEAB, 0.2% FA, and 50% ACN/0.2% FA. Samples were lyophilized and resuspended in 1% TFA/2% acetonitrile containing 12.5 fmol/µL yeast alcohol dehydrogenase. Quantitative LC/MS/MS was performed using a nanoAcquitiy UPLC system (Waters Corp) coupled to Thermo Scientific™ Orbitrap™ Fusion Lumos high resolution accurate mass tandem mass spectrometer via a nanoelectrospray ionization source. Data was analyzed with Proteome Discoverer 2.3 (Thermo Fisher Scientific™.) and MS/MS data searched against the *Chlamydia trachomatis* LGV L2 434 Bu reference database (NCBI:txid47472). Cdu1-Flag MS/MS data was analyzed with Mascot software (Matrix Science) using Trypsin/P specificity for N-terminal acetylation, lysine acetylation, lysine Ub, and S/T/Y phosphorylation identification. Analysis identified multiple acetylated and phosphorylated Cdu1 peptides and no Cdu1 ubiquitinated peptides. Data was viewed in Scaffold with Scaffold PTM (Scaffold Software).

Interferon gamma sensitivity assays

Ct sensitivities to interferon-gamma was assayed as previously described (Walsh et. al., 2022). Briefly, A549 cells were seeded in black 96-well clear-bottomed plates (Corning). The next day, cells were stimulated with 0 U/mL or 100 U/mL interferon gamma (IFNγ; Millipore, IF005) in DMEM supplemented with L-tryptophan (100 µg/mL). After 20 hours, cells were infected in technical duplicate with indicated *Chlamydia* strains at an MOI of 2. At 24 hours post-infection, plates were fixed with cold 4% PFA in PBS for 20 minutes. Samples were nuclear stained with Hoechst in PBS for 10 minutes and sealed using an aluminum adhesive (Thermo). Inclusions and host cell nuclei were imaged and quantified using the CellInsight CX5 High Content Screening platform (Thermo; CX51110). Relative bacterial infectivities were calculated as the number of inclusions divided by the total number of host nuclei for each sample. Interferon

907 sensitivity was calculated by normalizing the infectivities of each strain to it's "untreated" (-IFNγ)
908 control and expressed as a percentage.
909
910 **Isolation and imaging of *Chlamydia* inclusion extrusions**
911 HeLa cell monolayers (1.2 x 10^6 cells) were infected with Ct strains at MOIs of 0.8. At 48 hpi,
912 infected monolayers were imaged using an EVOS FL Cell Imaging System (ThermoFisher
913 Scientific) equipped with a 20x/0.4 NA objective and a CCD camera. Following imaging, growth
914 media was removed, cell monolayers washed with fresh growth media, and monolayers
915 incubated for an additional 4 hours at 37°C. At 52 hpi growth supernatants were collected and
916 transferred to Eppendorf tubes. Extrusions were enriched by centrifugation (1,500 rpm, 5 min)
917 and pellets (not always visible) containing extrusions were resuspended in 30 μL of 4%
918 Formaldehyde/PBS supplemented with Hoechst (2 μg/mL) and 0.2% Trypan Blue Solution
919 (Gibco, 0.4%). Extrusions were analyzed by plating 10 μL drops on a glass side (without
920 coverslips) and immediately imaged using an EVOS FL Cell Imaging System (ThermoFisher
921 Scientific) equipped with a 20x/0.4 NA objective and a CCD camera. Intact extrusions were
922 identified based on morphology, lacking nuclei, and being impermeable to trypan blue. Images
923 were opened in ImageJ (Schneider et al., 2012) and enumeration of inclusions and extrusions
924 was performed manually. The sizes of individual extrusions and inclusions were determined by
925 manually tracing a line around the perimeter of each extrusion and inclusion in ImageJ and
926 measuring perimeter length. All measurements were exported to Microsoft Excel. Data plots and
927 statistical analyses were done with Prism 9 (GraphPad) software. Datasets were analyzed for
928 significance using a paired student t-test.
929
930 **Image analysis**

Line scan profiles of Cdu1 co-localization with inclusion membrane proteins was performed with ImageJ (Schneider et al., 2012) by tracing a line through regions of interest and plotting fluorescent signal intensities with the Plot Profile function. Localization of CTL0480, recruitment of MYPT1, and association of Ub with Ct inclusions was performed manually from maximum projections in ImageJ. Assessment of F-actin recruitment to Ct inclusions was performed manually in ImageJ by projecting four to five sections in order to capture the entire inclusion. Redistribution of Golgi around the Ct inclusion was measured in ImageJ from maximum projections. The perimeters of individual inclusions were manually traced, and lengths measured. The length of dispersed Golgi was measured by tracing and measuring the length of the GM130 signal directly adjacent to each inclusion. Dispersed Golgi length was divided by inclusion perimeter length. All measurements were exported to Microsoft Excel for quantification. Data plots and statistical analyses were done with Prism 9 (GraphPad).

Quantification And Statistical Analysis

Quantifications were generated from three independent experiments and measurements derived from blinded images. Data plots and statistical analyses were done with Prism 9 (GraphPad) software. Datasets were analyzed for significance using a paired student t-test, one-way ANOVAs with a Student-Newman-Keuls post hoc test, or two-way ANOVAS with a Turkey post hoc test. Data graphs show means and error bars represent standard error. *p*-values less than 0.05 are defined as statistically significant. The indicated statistical test for each experiment can be found in the figure legends.

References

1. Abdelrahman YM, Belland RJ. 2005. The chlamydial developmental cycle. *FEMS Microbiol Rev* **29**:949–959. doi:10.1016/j.femsre.2005.03.002

2. Agaisse H, Derré I. 2013. A *C. trachomatis* cloning vector and the generation of *C. trachomatis* strains expressing fluorescent proteins under the control of a *C. trachomatis* promoter. *PLoS ONE* **8**:e57090. doi:10.1371/journal.pone.0057090

3. Albrecht M, Sharma CM, Reinhardt R, Vogel J, Rudel T. 2010. Deep sequencing-based discovery of the *Chlamydia trachomatis* transcriptome. *Nucleic Acids Res* **38**:868–877. doi:10.1093/nar/gkp1032

4. Alzhanov DT, Weeks SK, Burnett JR, Rockey DD. 2009. Cytokinesis is blocked in mammalian cells transfected with *Chlamydia trachomatis* gene CT223. *BMC Microbiol* **9**:2. doi:10.1186/1471-2180-9-2

5. Auer D, Hügelschäffer SD, Fischer AB, Rudel T. 2020. The chlamydial deubiquitinase Cdu1 supports recruitment of Golgi vesicles to the inclusion. *Cell Microbiol* **22**:e13136. doi:10.1111/cmi.13136

6. Bannantine JP, Griffiths RS, Viratyosin W, Brown WJ, Rockey DD. 2000. A secondary structure motif predictive of protein localization to the chlamydial inclusion membrane. *Cell Microbiol* **2**:35–47. doi:10.1046/j.1462-5822.2000.00029.x

7. Bauler LD, Hackstadt T. 2014. Expression and targeting of secreted proteins from *Chlamydia trachomatis*. *J Bacteriol* **196**:1325–1334. doi:10.1128/JB.01290-13

8. Berrow NS, Alderton D, Sainsbury S, Nettleship J, Assenberg R, Rahman N, Stuart DI, Owens RJ. 2007. A versatile ligation-independent cloning method suitable for high-

982 throughput expression screening applications. *Nucleic Acids Res* **35**:e45.
983 doi:10.1093/nar/gkm047
984
985 9. Bremm A, Freund SMV, Komander D. 2010. Lys11-linked ubiquitin chains adopt compact
986 conformations and are preferentially hydrolyzed by the deubiquitinase Cezanne. *Nat Struct*
987 *Mol Biol* **17**:939–947. doi:10.1038/nsmb.1873
988
989 10. Bugalhão JN, Mota LJ. 2019. The multiple functions of the numerous *Chlamydia trachomatis*
990 secreted proteins: the tip of the iceberg. *Microb Cell* **6**:414–449.
991 doi:10.15698/mic2019.09.691
992
993 11. Catic A, Misaghi S, Korbel GA, Ploegh HL. 2007. ElaD, a Deubiquitinating protease
994 expressed by *E. coli*. *PLoS ONE* **2**:e381. doi:10.1371/journal.pone.0000381
995
996 12. Chen C, Chen D, Sharma J, Cheng W, Zhong Y, Liu K, Jensen J, Shain R, Arulanandam B,
997 Zhong G. 2006. The hypothetical protein CT813 is localized in the *Chlamydia trachomatis*
998 inclusion membrane and is immunogenic in women urogenitally infected with *C.*
999 *trachomatis*. *Infect Immun* **74**:4826–4840. doi:10.1128/IAI.00081-06
1000
1001 13. Chen Y-S, Bastidas RJ, Saka HA, Carpenter VK, Richards KL, Plano GV, Valdivia RH.
1002 2014. The *Chlamydia trachomatis* type III secretion chaperone Slc1 engages multiple early
1003 effectors, including TepP, a tyrosine-phosphorylated protein required for the recruitment of
1004 CrkI-II to nascent inclusions and innate immune signaling. *PLoS Pathog* **10**:e1003954.
1005 doi:10.1371/journal.ppat.1003954
1006

14. Chin E, Kirker K, Zuck M, James G, Hybiske K. 2012. Actin recruitment to the *Chlamydia* inclusion is spatiotemporally regulated by a mechanism that requires host and bacterial factors. *PLoS ONE* **7**:e46949. doi:10.1371/journal.pone.0046949

15. Claessen JHL, Witte MD, Yoder NC, Zhu AY, Spooner E, Ploegh HL. 2013. Catch-and-release probes applied to semi-intact cells reveal ubiquitin-specific protease expression in *Chlamydia trachomatis* infection. *Chembiochem* **14**:343–352. doi:10.1002/cbic.201200701

16. Datta AB, Hura GL, Wolberger C. 2009. The structure and conformation of Lys63-linked tetraubiquitin. *J Mol Biol* **392**:1117–1124. doi:10.1016/j.jmb.2009.07.090

17. Dehoux P, Flores R, Dauga C, Zhong G, Subtil A. 2011. Multi-genome identification and characterization of chlamydiae-specific type III secretion substrates: the Inc proteins. *BMC Genomics* **12**:109. doi:10.1186/1471-2164-12-109

18. Dumoux M, Menny A, Delacour D, Hayward RD. 2015. A *Chlamydia* effector recruits CEP170 to reprogram host microtubule organization. *J Cell Sci* **128**:3420–3434. doi:10.1242/jcs.169318

19. Eddins MJ, Varadan R, Fushman D, Pickart CM, Wolberger C. 2007. Crystal structure and solution NMR studies of Lys48-linked tetraubiquitin at neutral pH. *J Mol Biol* **367**:204–211. doi:10.1016/j.jmb.2006.12.065

20. Fischer A, Harrison KS, Ramirez Y, Auer D, Chowdhury SR, Prusty BK, Sauer F, Dimond Z, Kisker C, Hefty PS, Rudel T. 2017. *Chlamydia trachomatis*-containing vacuole serves as

1032 deubiquitination platform to stabilize Mcl-1 and to interfere with host defense. *eLife* **6**.
1033 doi:10.7554/eLife.21465
1034
1035 21. Fiskin E, Bionda T, Dikic I, Behrends C. 2016. Global analysis of host and bacterial
1036 ubiquitinome in response to *Salmonella* Typhimurium infection. *Mol Cell* **62**:967–981.
1037 doi:10.1016/j.molcel.2016.04.015
1038
1039 22. Furtado AR, Essid M, Perrinet S, Balañá ME, Yoder N, Dehoux P, Subtil A. 2013. The
1040 chlamydial OTU domain-containing protein *Chla*OTU is an early type III secretion effector
1041 targeting ubiquitin and NDP52. *Cell Microbiol* **15**:2064–2079. doi:10.1111/cmi.12171
1042
1043 23. Gehre L, Gorgette O, Perrinet S, Prevost M-C, Ducatez M, Giebel AM, Nelson DE, Ball SG,
1044 Subtil A. 2016. Sequestration of host metabolism by an intracellular
1045 pathogen. *eLife* **5**:e12552. doi:10.7554/eLife.12552
1046
1047 24. Goedhart J, Luijsterburg MS. 2020. VolcaNoseR is a web app for creating, exploring,
1048 labeling and sharing volcano plots. *Sci Rep* **10**:20560. doi:10.1038/s41598-020-76603-3
1049
1050 25. Hackstadt T, Scidmore-Carlson MA, Shaw EI, Fischer ER. 1999. The *Chlamydia*
1051 *trachomatis* IncA protein is required for homotypic vesicle fusion. *Cell Microbiol* **1**:119–130.
1052 doi:10.1046/j.1462-5822.1999.00012.x
1053
1054 26. Haggerty CL, Gottlieb SL, Taylor BD, Low N, Xu F, Ness RB. 2010. Risk of sequelae after
1055 *Chlamydia trachomatis* genital infection in women. *J Infect Dis* **201 Suppl 2**:S134-55.
1056 doi:10.1086/652395
1057

1058 27. Haines A, Wesolowski J, Ryan NM, Monteiro-Brás T, Paumet F. 2021. Cross Talk between
1059 ARF1 and RhoA Coordinates the Formation of Cytoskeletal Scaffolds during *Chlamydia*
1060 *Infection*. *MBio* **12**:e0239721. doi:10.1128/mBio.02397-21
1061
1062 28. Hausman JM, Kenny S, Iyer S, Babar A, Qiu J, Fu J, Luo Z-Q, Das C. 2020. The Two
1063 Deubiquitinating Enzymes from *Chlamydia trachomatis* Have Distinct Ubiquitin Recognition
1064 Properties. *Biochemistry* **59**:1604–1617. doi:10.1021/acs.biochem.9b01107
1065
1066 29. Huang DW, Sherman BT, Lempicki RA. 2009a. Bioinformatics enrichment tools: paths
1067 toward the comprehensive functional analysis of large gene lists. *Nucleic Acids Res* **37**:1–
1068 13. doi:10.1093/nar/gkn923
1069
1070 30. Huang DW, Sherman BT, Lempicki RA. 2009b. Systematic and integrative analysis of large
1071 gene lists using DAVID bioinformatics resources. *Nat Protoc* **4**:44–57.
1072 doi:10.1038/nprot.2008.211
1073
1074 31. Hybiske K, Stephens RS. 2007. Mechanisms of host cell exit by the intracellular bacterium
1075 *Chlamydia*. *Proc Natl Acad Sci USA* **104**:11430–11435. doi:10.1073/pnas.0703218104
1076
1077 32. Iyer S, Das C. 2021. The unity of opposites: Strategic interplay between bacterial effectors
1078 to regulate cellular homeostasis. *J Biol Chem* **297**:101340. doi:10.1016/j.jbc.2021.101340
1079
1080 33. Jeong KC, Sexton JA, Vogel JP. 2015. Spatiotemporal regulation of a *Legionella*
1081 *pneumophila* T4SS substrate by the metaeffector SidJ. *PLoS Pathog* **11**:e1004695.
1082 doi:10.1371/journal.ppat.1004695
1083

34. Jones RM, Wu H, Wentworth C, Luo L, Collier-Hyams L, Neish AS. 2008. *Salmonella avra* coordinates suppression of host immune and apoptotic defenses via JNK pathway blockade. *Cell Host Microbe* **3**:233–244. doi:10.1016/j.chom.2008.02.016

35. Kędzior M, Bastidas RJ. 2019. Forward and reverse genetic analysis of *Chlamydia*. *Methods Mol Biol* **2042**:185–204. doi:10.1007/978-1-4939-9694-0_13

36. Kokes M, Dunn JD, Granek JA, Nguyen BD, Barker JR, Valdivia RH, Bastidas RJ. 2015. Integrating chemical mutagenesis and whole-genome sequencing as a platform for forward and reverse genetic analysis of *Chlamydia*. *Cell Host Microbe* **17**:716–725. doi:10.1016/j.chom.2015.03.014

37. Komander D, Clague MJ, Urbé S. 2009a. Breaking the chains: structure and function of the deubiquitinases. *Nat Rev Mol Cell Biol* **10**:550–563. doi:10.1038/nrm2731

38. Komander D, Reyes-Turcu F, Licchesi JDF, Odenwaelder P, Wilkinson KD, Barford D. 2009b. Molecular discrimination of structurally equivalent Lys 63-linked and linear polyubiquitin chains. *EMBO Rep* **10**:466–473. doi:10.1038/embor.2009.55

39. Komander D, Rape M. 2012. The ubiquitin code. *Annu Rev Biochem* **81**:203–229. doi:10.1146/annurev-biochem-060310-170328

40. Kubori T, Shinzawa N, Kanuka H, Nagai H. 2010. *Legionella* metaeffector exploits host proteasome to temporally regulate cognate effector. *PLoS Pathog* **6**:e1001216. doi:10.1371/journal.ppat.1001216

41. Kubori T, Kitao T, Nagai H. 2019. Emerging insights into bacterial deubiquitinases. *Curr Opin Microbiol* **47**:14–19. doi:10.1016/j.mib.2018.10.001

42. Kumar Y, Valdivia RH. 2008. Actin and intermediate filaments stabilize the *Chlamydia trachomatis* vacuole by forming dynamic structural scaffolds. *Cell Host Microbe* **4**:159–169. doi:10.1016/j.chom.2008.05.018

43. Kunz TC, Götz R, Sauer M, Rudel T. 2019. Detection of *Chlamydia* developmental forms and secreted effectors by expansion microscopy. *Front Cell Infect Microbiol* **9**:276. doi:10.3389/fcimb.2019.00276

44. Lee JK, Enciso GA, Boassa D, Chander CN, Lou TH, Pairawan SS, Guo MC, Wan FYM, Ellisman MH, Sütterlin C, Tan M. 2018. Replication-dependent size reduction precedes differentiation in *Chlamydia trachomatis*. *Nat Commun* **9**:45. doi:10.1038/s41467-017-02432-0

45. Le Negrate G, Krieg A, Faustin B, Loeffler M, Godzik A, Krajewski S, Reed JC. 2008. ChlaDub1 of *Chlamydia trachomatis* suppresses NF-κB activation and inhibits IκBα ubiquitination and degradation. *Cell Microbiol* **10**:1879–1892. doi:10.1111/j.1462-5822.2008.01178.x

46. Li J, Chai Q-Y, Liu CH. 2016. The ubiquitin system: a critical regulator of innate immunity and pathogen-host interactions. *Cell Mol Immunol* **13**:560–576. doi:10.1038/cmi.2016.40

47. Li Z, Chen C, Chen D, Wu Y, Zhong Y, Zhong G. 2008. Characterization of fifty putative inclusion membrane proteins encoded in the *Chlamydia trachomatis* genome. *Infect Immun* **76**:2746–2757. doi:10.1128/IAI.00010-08

48. Lowden NM, Yeruva L, Johnson CM, Bowlin AK, Fisher DJ. 2015. Use of aminoglycoside 3' adenyltransferase as a selection marker for *Chlamydia trachomatis* intron-mutagenesis and in vivo intron stability. *BMC Res Notes* **8**:570. doi:10.1186/s13104-015-1542-9

49. Lutter EI, Martens C, Hackstadt T. 2012. Evolution and conservation of predicted inclusion membrane proteins in *Chlamydiae*. *Comp Funct Genomics* **2012**:362104. doi:10.1155/2012/362104

50. Lutter EI, Barger AC, Nair V, Hackstadt T. 2013. *Chlamydia trachomatis* inclusion membrane protein CT228 recruits elements of the myosin phosphatase pathway to regulate release mechanisms. *Cell Rep* **3**:1921–1931. doi:10.1016/j.celrep.2013.04.027

51. Makarova KS, Aravind L, Koonin EV. 2000. A novel superfamily of predicted cysteine proteases from eukaryotes, viruses and *Chlamydia pneumoniae*. *Trends Biochem Sci* **25**:50–52. doi:10.1016/s0968-0004(99)01530-3

52. Meier K, Jachmann LH, Türköz G, Babu Sait MR, Pérez L, Kepp O, Valdivia RH, Kroemer G, Sixt BS. 2023. The *Chlamydia* effector CpoS modulates the inclusion microenvironment and restricts the interferon response by acting on Rab35. *MBio* **14**:e0319022. doi:10.1128/mbio.03190-22

53. Meier K, Jachmann LH, Pérez L, Kepp O, Valdivia RH, Kroemer G, Sixt BS. 2022. The *Chlamydia* protein CpoS modulates the inclusion microenvironment and restricts the interferon response by acting on Rab35. *BioRxiv*. doi:10.1101/2022.02.18.481055

54. Misaghi S, Balsara ZR, Catic A, Spooner E, Ploegh HL, Starnbach MN. 2006. *Chlamydia trachomatis*-derived deubiquitinating enzymes in mammalian cells during infection. *Mol Microbiol* **61**:142–150. doi:10.1111/j.1365-2958.2006.05199.x

55. Mittal R, Peak-Chew S-Y, McMahon HT. 2006. Acetylation of MEK2 and IκB kinase (IKK) activation loop residues by YopJ inhibits signaling. *Proc Natl Acad Sci USA* **103**:18574–18579. doi:10.1073/pnas.0608995103

56. Mital J, Miller NJ, Fischer ER, Hackstadt T. 2010. Specific chlamydial inclusion membrane proteins associate with active Src family kinases in microdomains that interact with the host microtubule network. *Cell Microbiol***12**:1235–1249. doi:10.1111/j.1462-5822.2010.01465.x

57. Mizuno E, Kitamura N, Komada M. 2007. 14-3-3-dependent inhibition of the deubiquitinating activity of UBPY and its cancellation in the M phase. *Exp Cell Res* **313**:3624–3634. doi:10.1016/j.yexcr.2007.07.028

58. Moulder JW. 1991. Interaction of *Chlamydiae* and host cells in vitro. *Microbiol Rev* **55**:143–190.

59. Mukherjee S, Keitany G, Li Y, Wang Y, Ball HL, Goldsmith EJ, Orth K. 2006. *Yersinia* YopJ acetylates and inhibits kinase activation by blocking phosphorylation. *Science* **312**:1211–1214. doi:10.1126/science.1126867

60. Neunuebel MR, Chen Y, Gaspar AH, Backlund PS, Yergey A, Machner MP. 2011. De-AMPylation of the small GTPase Rab1 by the pathogen *Legionella pneumophila*. *Science* **333**:453–456. doi:10.1126/science.1207193

61. Nguyen BD, Valdivia RH. 2012. Virulence determinants in the obligate intracellular pathogen *Chlamydia trachomatis* revealed by forward genetic approaches. *Proc Natl Acad Sci USA* **109**:1263–1268. doi:10.1073/pnas.1117884109

62. Nguyen PH, Lutter EI, Hackstadt T. 2018. *Chlamydia trachomatis* inclusion membrane protein MrcA interacts with the inositol 1,4,5-trisphosphate receptor type 3 (ITPR3) to regulate extrusion formation. *PLoS Pathog***14**:e1006911. doi:10.1371/journal.ppat.1006911

63. Ohtake F, Tsuchiya H. 2017. The emerging complexity of ubiquitin architecture. *J Biochem* **161**:125–133. doi:10.1093/jb/mvw088

64. Pannekoek Y, Spaargaren J, Langerak AAJ, Merks J, Morré SA, van der Ende A. 2005. Interrelationship between polymorphisms of *incA*, fusogenic properties of *Chlamydia trachomatis* strains, and clinical manifestations in patients in The Netherlands. *J Clin Microbiol* **43**:2441–2443. doi:10.1128/JCM.43.5.2441-2443.2005

65. Peng J, Schwartz D, Elias JE, Thoreen CC, Cheng D, Marsischky G, Roelofs J, Finley D, Gygi SP. 2003. A proteomics approach to understanding protein ubiquitination. *Nat Biotechnol* **21**:921–926. doi:10.1038/nbt849

66. Pruneda JN, Durkin CH, Geurink PP, Ovaa H, Santhanam B, Holden DW, Komander D. 2016. The Molecular Basis for Ubiquitin and Ubiquitin-like Specificities in Bacterial Effector Proteases. *Mol Cell* **63**:261–276. doi:10.1016/j.molcel.2016.06.015

67. Pruneda JN, Bastidas RJ, Bertsoulaki E, Swatek KN, Santhanam B, Clague MJ, Valdivia RH, Urbé S, Komander D. 2018. A *Chlamydia* effector combining deubiquitination and acetylation activities induces Golgi fragmentation. *Nat Microbiol* **3**:1377–1384. doi:10.1038/s41564-018-0271-y

68. Reiley W, Zhang M, Wu X, Granger E, Sun S-C. 2005. Regulation of the deubiquitinating enzyme CYLD by IκB kinase gamma-dependent phosphorylation. *Mol Cell Biol* **25**:3886–3895. doi:10.1128/MCB.25.10.3886-3895.2005

69. Roan NR, Gierahn TM, Higgins DE, Starnbach MN. 2006. Monitoring the T cell response to genital tract infection. *Proc Natl Acad Sci USA* **103**:12069–12074. doi:10.1073/pnas.0603866103

70. Rockey DD, Scidmore MA, Bannantine JP, Brown WJ. 2002. Proteins in the chlamydial inclusion membrane. *Microbes Infect* **4**:333–340. doi:10.1016/s1286-4579(02)01546-0

71. Ronau JA, Beckmann JF, Hochstrasser M. 2016. Substrate specificity of the ubiquitin and Ubl proteases. *Cell Res* **26**:441–456. doi:10.1038/cr.2016.38

72. Rytkönen A, Poh J, Garmendia J, Boyle C, Thompson A, Liu M, Freemont P, Hinton JCD, Holden DW. 2007. SseL, a *Salmonella* deubiquitinase required for macrophage killing and virulence. *Proc Natl Acad Sci USA***104**:3502–3507. doi:10.1073/pnas.0610095104

73. Saeki Y. 2017. Ubiquitin recognition by the proteasome. *J Biochem* **161**:113–124. doi:10.1093/jb/mvw091

74. Schneider CA, Rasband WS, Eliceiri KW. 2012. NIH Image to ImageJ: 25 years of image analysis. *Nat Methods* **9**:671–675. doi:10.1038/nmeth.2089

75. Schubert AF, Nguyen JV, Franklin TG, Geurink PP, Roberts CG, Sanderson DJ, Miller LN, Ovaa H, Hofmann K, Pruneda JN, Komander D. 2020. Identification and characterization of diverse OTU deubiquitinases in bacteria. *EMBO J* **39**:e105127. doi:10.15252/embj.2020105127

76. Shaw JH, Key CE, Snider TA, Sah P, Shaw EI, Fisher DJ, Lutter EI. 2018. Genetic Inactivation of *Chlamydia trachomatis* Inclusion Membrane Protein CT228 Alters MYPT1 Recruitment, Extrusion Production, and Longevity of Infection. *Front Cell Infect Microbiol* **8**:415. doi:10.3389/fcimb.2018.00415

77. Sheedlo MJ, Qiu J, Tan Y, Paul LN, Luo Z-Q, Das C. 2015. Structural basis of substrate recognition by a bacterial deubiquitinase important for dynamics of phagosome ubiquitination. *Proc Natl Acad Sci USA* **112**:15090–15095. doi:10.1073/pnas.1514568112

78. Sixt BS, Bastidas RJ, Finethy R, Baxter RM, Carpenter VK, Kroemer G, Coers J, Valdivia RH. 2017. The *Chlamydia trachomatis* Inclusion Membrane Protein CpoS Counteracts STING-Mediated Cellular Surveillance and Suicide Programs. *Cell Host Microbe* **21**:113–121. doi:10.1016/j.chom.2016.12.002

79. Smith EP, Cotto-Rosario A, Borghesan E, Held K, Miller CN, Celli J. 2020. Epistatic Interplay between Type IV Secretion Effectors Engages the Small GTPase Rab2 in the *Brucella* Intracellular Cycle. *MBio* **11**. doi:10.1128/mBio.03350-19

80. Suchland RJ, Rockey DD, Bannantine JP, Stamm WE. 2000. Isolates of *Chlamydia trachomatis* that occupy nonfusogenic inclusions lack IncA, a protein localized to the inclusion membrane. *Infect Immun* **68**:360–367. doi:10.1128/IAI.68.1.360-367.2000

81. Swatek KN, Komander D. 2016. Ubiquitin modifications. *Cell Res* **26**:399–422. doi:10.1038/cr.2016.39

82. Tenno T, Fujiwara K, Tochio H, Iwai K, Morita EH, Hayashi H, Murata S, Hiroaki H, Sato M, Tanaka K, Shirakawa M. 2004. Structural basis for distinct roles of Lys63- and Lys48-linked polyubiquitin chains. *Genes Cells***9**:865–875. doi:10.1111/j.1365-2443.2004.00780.x

83. Urbanus ML, Quaile AT, Stogios PJ, Morar M, Rao C, Di Leo R, Evdokimova E, Lam M, Oatway C, Cuff ME, Osipiuk J, Michalska K, Nocek BP, Taipale M, Savchenko A, Ensminger AW. 2016. Diverse mechanisms of metaeffector activity in an intracellular bacterial pathogen, *Legionella pneumophila*. *Mol Syst Biol* **12**:893. doi:10.15252/msb.20167381

84. Varadan R, Walker O, Pickart C, Fushman D. 2002. Structural properties of polyubiquitin chains in solution. *J Mol Biol* **324**:637–647. doi:10.1016/s0022-2836(02)01198-1

85. Vozandychova V, Stojkova P, Hercik K, Rehulka P, Stulik J. 2021. The Ubiquitination System within Bacterial Host-Pathogen Interactions. *Microorganisms* **9**. doi:10.3390/microorganisms9030638

86. Walsh SC, Reitano JR, Dickinson MS, Kutsch M, Hernandez D, Barnes AB, Schott BH, Wang L, Ko DC, Kim SY, Valdivia RH, Bastidas RJ, Coers J. 2022. The bacterial effector

GarD shields *Chlamydia trachomatis* inclusions from RNF213-mediated ubiquitylation and destruction. *Cell Host Microbe*. doi:10.1016/j.chom.2022.08.008

87. Wang X, Hybiske K, Stephens RS. 2018. Direct visualization of the expression and localization of chlamydial effector proteins within infected host cells. *Pathog Dis* **76**. doi:10.1093/femspd/fty011

88. Weber MM, Bauler LD, Lam J, Hackstadt T. 2015. Expression and localization of predicted inclusion membrane proteins in *Chlamydia trachomatis*. *Infect Immun* **83**:4710–4718. doi:10.1128/IAI.01075-15

89. Weeks SD, Grasty KC, Hernandez-Cuebas L, Loll PJ. 2009. Crystal structures of Lys-63-linked tri- and di-ubiquitin reveal a highly extended chain architecture. *Proteins* **77**:753–759. doi:10.1002/prot.22568

90. Wesolowski J, Weber MM, Nawrotek A, Dooley CA, Calderon M, St Croix CM, Hackstadt T, Cherfils J, Paumet F. 2017. *Chlamydia* hijacks ARF gtpases to coordinate microtubule posttranslational modifications and golgi complex positioning. *MBio* **8**. doi:10.1128/mBio.02280-16

91. Zadora PK, Chumduri C, Imami K, Berger H, Mi Y, Selbach M, Meyer TF, Gurumurthy RK. 2019. Integrated Phosphoproteome and Transcriptome Analysis Reveals *Chlamydia*-Induced Epithelial-to-Mesenchymal Transition in Host Cells. *Cell Rep* **26**:1286-1302.e8. doi:10.1016/j.celrep.2019.01.006

92. Zhou Y, Zhou B, Pache L, Chang M, Khodabakhshi AH, Tanaseichuk O, Benner C, Chanda SK. 2019. Metascape provides a biologist-oriented resource for the analysis of systems-level datasets. *Nat Commun* **10**:1523. doi:10.1038/s41467-019-09234-6

93. Zuck M, Ellis T, Venida A, Hybiske K. 2017. Extrusions are phagocytosed and promote *Chlamydia* survival within macrophages. *Cell Microbiol* **19**. doi:10.1111/cmi.12683

94. Zuck M, Sherrid A, Suchland R, Ellis T, Hybiske K. 2016. Conservation of extrusion as an exit mechanism for *Chlamydia*. *Pathog Dis* **74**. doi:10.1093/femspd/ftw093

Figures

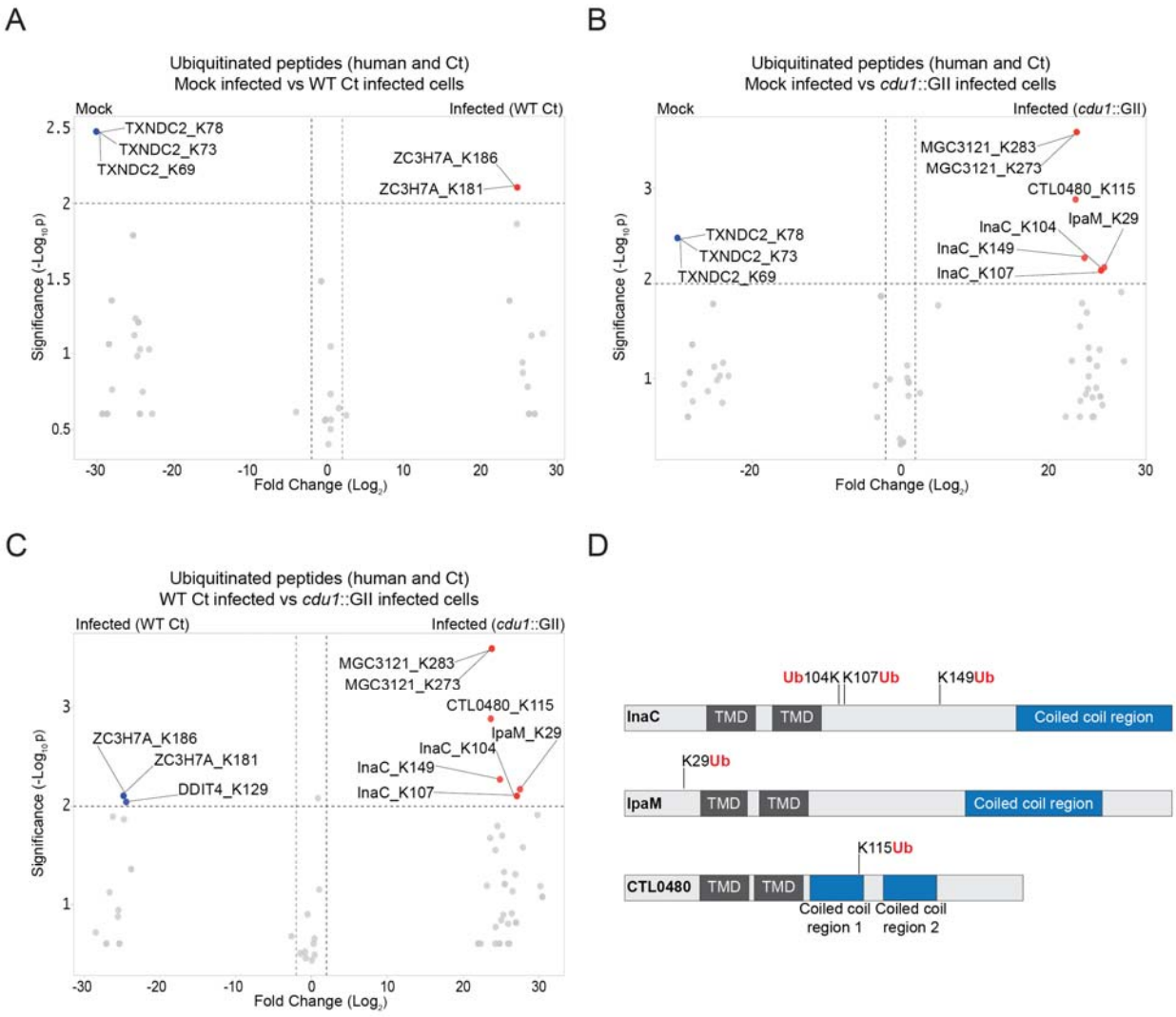

Figure 1

The *C. trachomatis* inclusion membrane proteins InaC, IpaM, and CTL0480 are ubiquitinated in the absence of Cdu1. (A-C) Volcano plots (pairwise comparisons) of the relative abundance of human and Ct ubiquitinated peptides.**(A)** Mock infected HeLa cells versus HeLa cells infected with WT Ct (L2 434 Bu pBOMB) (24 hpi). **(B)** Mock infected HeLa cells versus HeLa cells infected with a *cdu1* null strain (*cdu1*::GII pBOMB) (24 hpi) **(C)** HeLa cells infected with WT Ct (24 hpi) versus HeLa cells infected with a *cdu1* null strain (24 hpi). Significance values were interpolated from 3 independent biological replicates. Ubiquitinated proteins were enriched with magnetic TUBE 1 beads (binds to polyubiquitinated proteins) and peptides identified by quantitative LC MS/MS analysis. Three Ct inclusion membrane proteins, InaC, IpaM, and CTL0480 were differentially ubiquitinated in the absence of Cdu1. **(D)** InaC was ubiquitinated at K104, K107, and K149, IpaM at K290, and CTL0480 at K115 in the absence of Cdu1. TMD: Transmembrane domain. Numbering corresponds to amino acids in the protein sequence of each respective inclusion membrane protein.

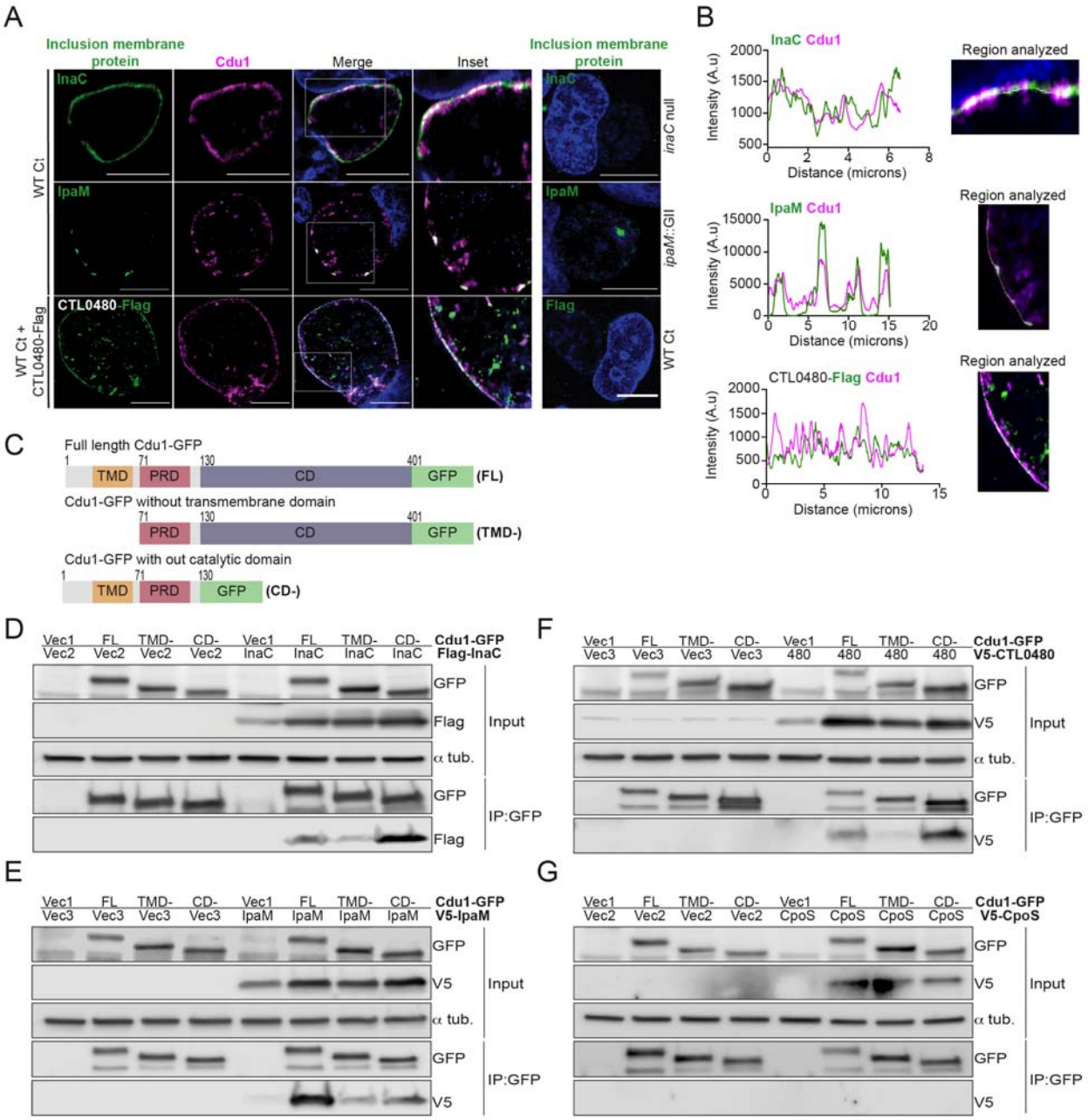

Figure 2

Cdu1 associates with InaC, IpaM, and CTL0480. (A) Co-localization of Cdu1(magenta) with endogenous InaC (green), IpaM (green), and ectopically expressed CTL0480-Flag (green) at the Ct (L2) inclusion membrane of HeLa cells infected for 24 h. HeLa cells infected with an *inaC* null strain (M407), an *ipaM* null strain (*ipaM*::GII), and WT Ct (L2 434 Bu pBOMB) were used as controls for antibody specificity. DNA stained with Hoechst is shown in blue. Scale bar: 10µm. Images are representative of multiple images captured across three independent replicates. **(B)** Line scan profiles of fluorescent signal intensities displayed in (A) showing co-localization of fluorescence intensities for endogenous Cdu1 with endogenous InaC and IpaM, and with CTL0480-Flag along the L2 inclusion membrane. **(C)** Schematic of Cdu1-GFP(C) (L2) fusion (Cdu1-GFP) and Cdu1-GFP variants used in co-transfections of HEK 293 cells. GFP: Green fluorescent protein. TMD: Transmembrane domain. PRD: Proline rich domain. CD: Catalytic

domain. FL: Full length. TMD-: Cdu1-GFP variant lacking TMD domain. CD-: Cdu1-GFP variant lacking CD domain. **(D-G)** Western blot analysis of GFP immunoprecipitates from HEK 293 cells co-transfected with mammalian plasmids expressing: Cdu1-GFP variants and **(D)** truncated 3XFlag(N)-InaC (D/UW-3/CX CT813, amino acids 96-264), **(E)** V5(N)-IpaM (L2, full length), **(F)** V5(N)-CTL0480 (L2, full length), and **(G)** V5(N)-CpoS (L2, full length). Vec1: Empty pOPINN-GFP vector. Vec2: Empty pDEST53 vector. Vec3: Empty pcDNA^{TM}3.1/nV5-DEST vector. Western blot images are representative from two independent experiments.

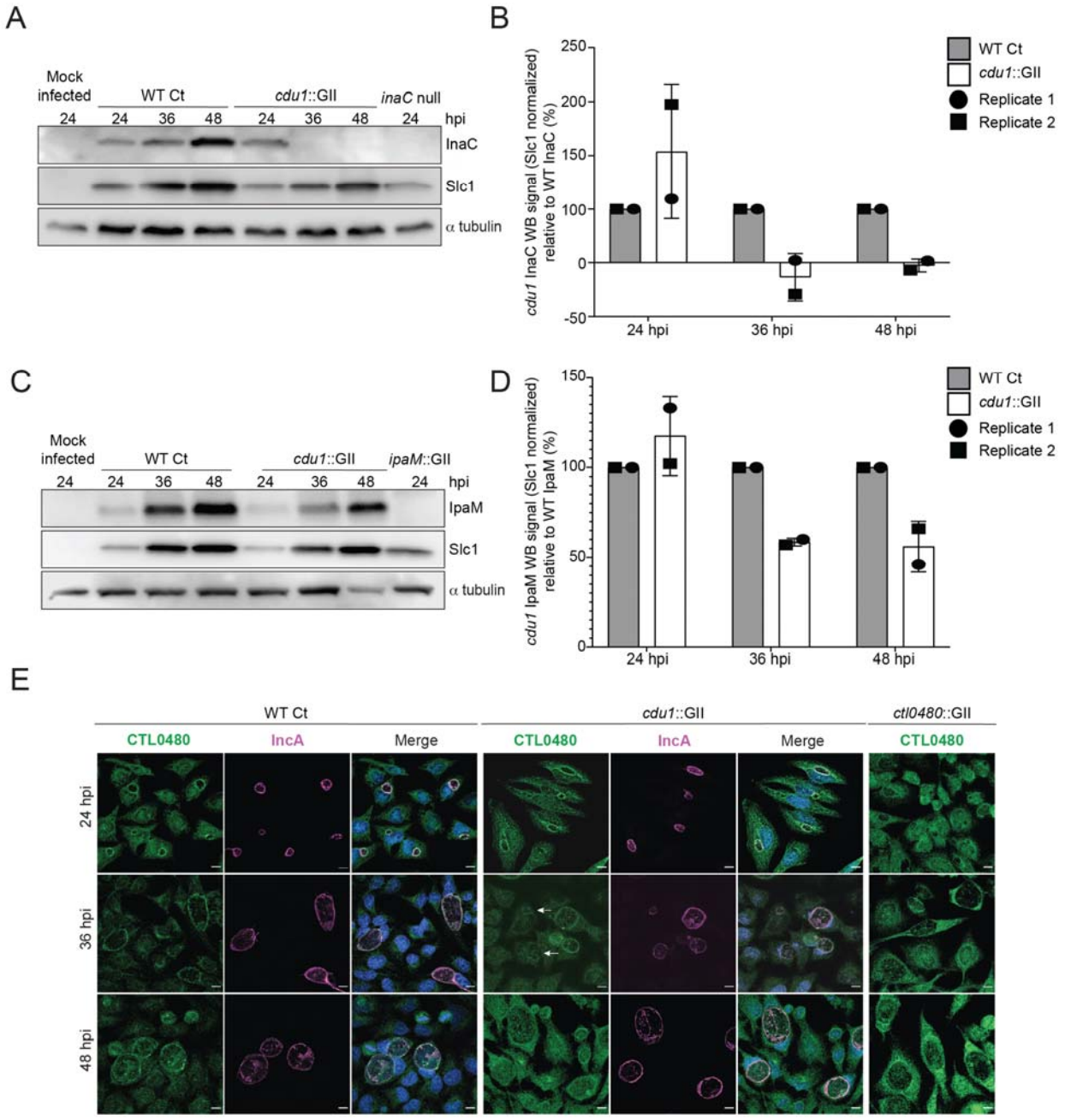

Figure 3

Cdu1 stabilizes InaC, IpaM, and CTL0480. (A) Western blot analysis of endogenous InaC in HeLa cells infected for 24, 36, and 48 hours with Wt Ct (L2 pBOMB), *cdu1* null (*cdu1*::GII pBOMB), and *inaC* null (M407) strains. Ct Slc1 and human alpha tubulin were used to determine Ct burdens and equal loading of protein extracts respectively. Western blot images are representative of 2 independent experiments. **(B)** Quantification of InaC abundance (InaC western blot signal from (A)) normalized to Slc1 western blot signal (from panel A) in Hela cells infectedwith a *cdu1* null strain, relative to normalized InaC abundance in Hela cells infected with Wt Ct. **(C)** Western blot analysis of endogenous IpaM in HeLa cells infected for 24, 36, and 48 hours with Wt Ct, *cdu1* null, and *ipam* null (*ipam*::GII) strains. Western blot images are representative of 2 independent experiments. **(D)** Quantification of normalized IpaM abundance

(from (C) in Hela cells infectedwith a *cdu1* null strain, relative to normalized IpaM abundance in Hela cells infected with Wt Ct. **(E)** Localization of CTL0480 during Ct infection of HeLa cells at 24, 36, and 48 hpi. CTL0480 signal (green) co-localizes with the inclusion membrane protein IncA (magenta) at the Ct inclusion membrane. Arrowheads highlight *cdu1* null inclusions lacking CTL0480 at 36 hpi. DNA stained with Hoechst is shown in blue. Scale bar: 10µm. Quantification of MYPT1 localization at inclusion membranes can be found in Supplemental Figure 5

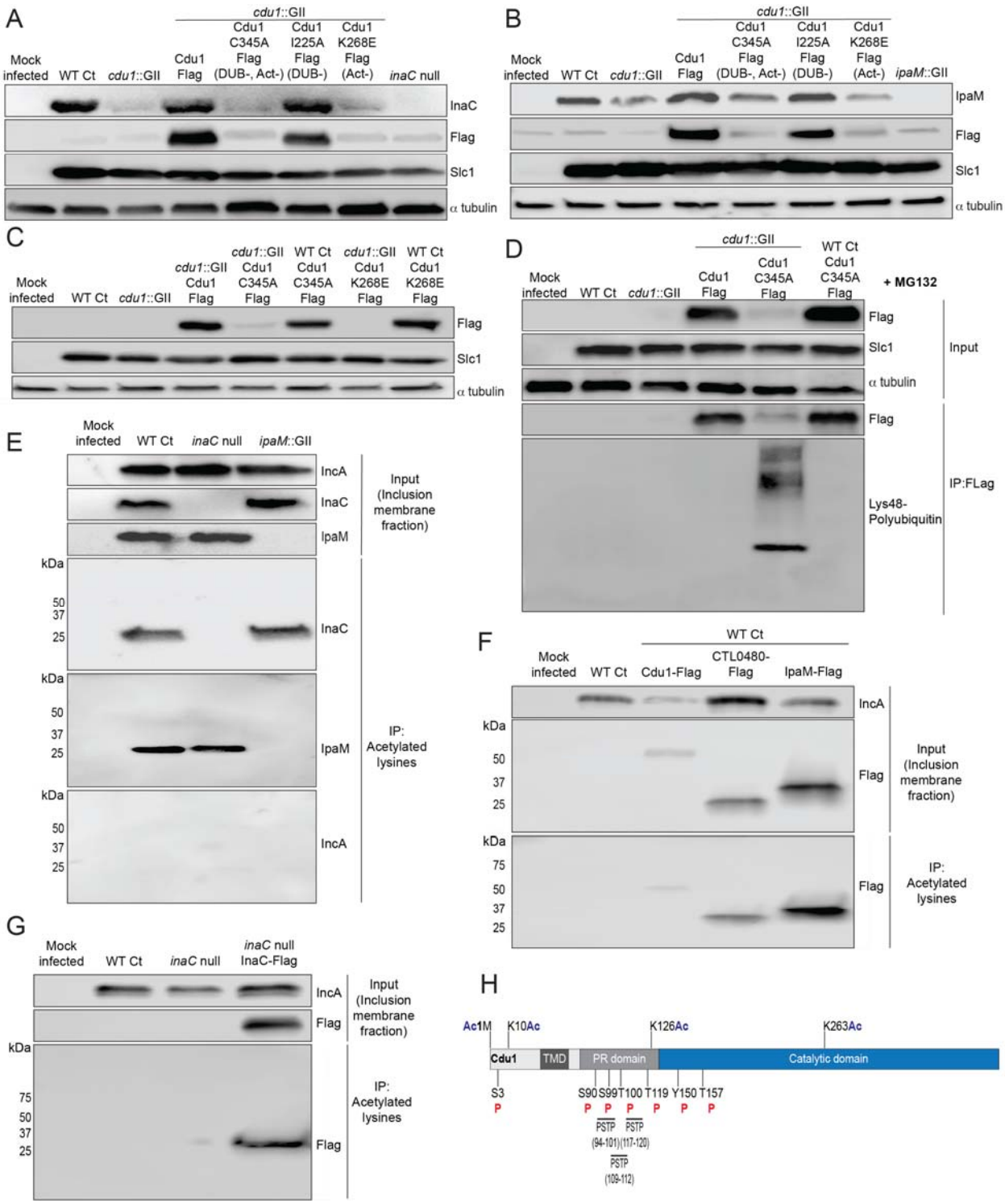

Figure 4

The acetylase activity of Cdu1 is required to stabilize Cdu1, InaC, and IpaM. (A) Western blot analysis of endogenous InaC and Cdu1-Flag catalytic variants expressed from a plasmid (pBOMB). HeLa cells were infected for 36 hours with WT Ct (L2 434 Bu pBOMB), a *cdu1* null strain (*cdu1*::GII pBOMB), and *cdu1* null strains expressing wild type Cdu1-Flag and the Cdu1 variants C345A-Flag (catalytic inactive), I225A-Flag (DUB deficient), and K268E-Flag (Act

deficient). Cdu1-Flag variants were expressed from a pBOMB shuttle plasmid. Protein lysates from HeLa cells infected with an *inaC* null (M407) strain were used to control for the specificity of anti-InaC antibodies. Western blot images are representative of two independent experiments. **(B)** Western blot analysis of endogenous IpaM and Cdu1-FLAG variants in crude extracts of HeLa cells infected for 48 hours with the same strains as describe in (A). Infection of HeLa cells with *ipaM*::GII was used to test for the specificity of the anti-IpaM antibody. Western blot images are representative of two independent experiments. **(C)** Western blot analysis of Cdu1^{C345A}-Flag (catalytic inactive) and Cdu1^{K268E}-Flag (Act deficient) expressed in a *cdu1* null strain or WT Ct (L2 434 Bu) background after infection of HeLa cells for 24 hours. Both Cdu1 variants are stabilized by Cdu1 expressed in WT Ct. **(D)** Western blot analysis of Cdu1-Flag and Cdu1^{C345A}-Flag expressed in a *cdu1* null strain and Cdu1^{C345A}-Flag expressed in WT Ct (L2 434 Bu) following immunoprecipitation (anti-Flag) from HeLa cell extracts after infection for 24 hours and treatment with MG132 (25 μM, 5 hours). Western blot image is a representative blot from at least three independent experiments. **(E)** Western blot analysis of endogenous InaC and IpaM following immunoprecipitation of inclusion membrane enriched subcellular fractions (24hpi) with anti acetylated lysine antibodies. Western blot image is representative of two independent experiments. **(F)** Western blot analysis (Flag WB) of acetylated lysine immunoprecipitates generated from inclusion membrane enriched subcellular fractions (40 hpi) derived from HeLa cells infected with WT Ct strains expressing Cdu1-Flag, CTL0480-Flag, or IpaM-Flag. Western blot image is representative of two independent experiments. **(G)** WB of acetylated lysine immunoprecipitates of inclusion membrane enriched fractions (24 hpi) of HeLa cells infected with WT Ct and with an *inaC* null strain (M407) expressing InaC-Flag. Western blot image is representative of two independent experiments. **(H)** The initiator methionine, Lys10, Lys126, and Lys263 of Cdu1 are acetylated by 24 hpi. One tyrosine (Y) residue and multiple serine (S) and threonine (T) residues in Cdu1 are also phosphorylated during Ct infection of HeLa cells (24 hpi). Three PX(S/T)P MAPK phosphorylation consensus sequence motifs were identified in the proline rich domain of Cdu1. Modified residues were identified by quantitative LC MS/MS analysis of immunoprecipitated Cdu1-Flag across 3 independent biological replicates. TMD: Transmembrane domain. PR: Proline rich. PSTP: PX(S/T)P motifs. Ac: Acetylation. P: Phosphorylation. Numbering corresponds to amino acids in Cdu1 protein sequence.

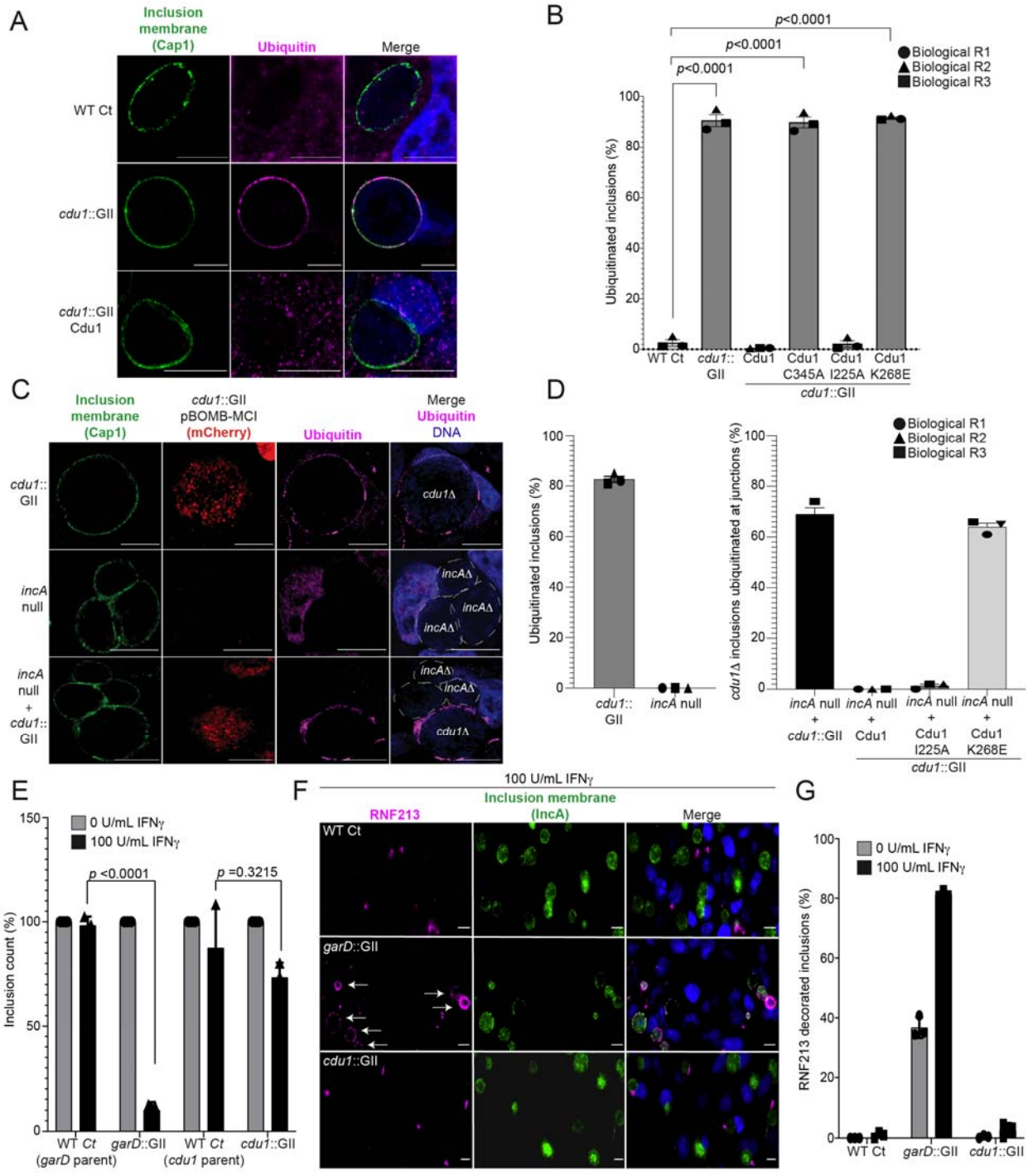

Figure 5

The DUB activity of Cdu1 is not required for blocking the ubiquitination of inclusion membranes and Cdu1 is not required for protection against IFNγ mediated cellular immunity. (A) Representative images of Ct inclusions decorated with ubiquitin during infection of HeLa cells with a *cdu1*::GII strain for 24 hours. Representative images of infected Hela cells used for quantification of ubiquitin decorated inclusions in (B) are shown in Supplemental Figure 6A. Antisera against the membrane protein Cap1 (green) was used to mark inclusion

membranes. DNA stained with Hoechst is shown in blue. Scale bar: 10µm. **(B)** Quantification of ubiquitinated inclusions as shown in (A). The Ub fluorescent signal was used to determine the number of infected cells with Ub decorated inclusions. The total number of ubiquitinated inclusions was divided by the total number of inclusions analyzed (defined by Cap1 staining). 87%, 86%, and 91% of inclusions were decorated with Ub in HeLa cells infected with a *cdu1* null strain and *cdu1* null strains expressing Cdu1^{C345A} (DUB-, Act-), and Cdu1^{K268E} (Act-) variants respectively. Representative images (panel (A) and Supplemental Figure 6A) and quantification of ubiquitinated inclusions were obtained from inclusions imaged in 10 fields across 3 independent biological replicates for each strain. *p* values were determined by a student paired t-test. **(C)** Representative images of HeLa cells co-infected with *cdu1*::GII (*cdu1Δ*) and *incA* null (*incA*Δ, M923) strains at 24 hpi. IncA-deficient inclusions do not fuse with other inclusions. In co-infected cells, Cdu1 present on the inclusion membranes of *incAΔ* strains did not block ubiquitination events at or near the inclusion membranes of neighboring *cdu1Δ* strains (mCherry signal from pBOMB4-MCI plasmid). Representative images of Hela cells infected with strains quantified in (D) are shown in Supplemental Figure 6B. DNA stained with Hoechst is shown in blue. Scale bar: 10µm. **(D)** Quantification of *cdu1Δ* inclusions as shown in (C) in which ubiquitination events are observed in regions of *cdu1Δ* inclusion membranes that are in direct apposition to *incAΔ* inclusion membranes (junctions). The total number of *cdu1Δ* inclusions ubiquitinated at inclusion junctions was divided by the total number of inclusions analyzed (Cap1 staining). 66% and 61% of *cdu1Δ* inclusions were decorated with Ub at junctions in HeLa cells co-infected with *incAΔ* and *cdu1Δ* strains or with *incAΔ* and a *cdu1Δ* strain ectopically expressing Cdu1^{K268E} (Act-) respectively. Representative images (panel (C) and Supplemental Figure 6B) and quantification of *cdu1Δ* inclusions ubiquitinated at junctions are derived from inclusions imaged in 6 fields across 3 independent biological replicates for each condition. *p* values were determined by a student paired t-test. **(E)** Quantification of Ct inclusion production during infection of unprimed and IFNγ-primed (100 U/mL) A549 cells at 24 hours post infection. Inclusions were quantified by high-content imaging analysis. Plot reflects inclusion counts across 9 fields of view and 3 independent biological replicates. Inclusion counts by each strain in unprimed A549 cells were set to 100%. Inclusion counts resulting from *cdu1*::GII and *garD*::GII strains were normalized to corresponding parental Ct inclusion (100%) counts in unprimed cells. P-values were calculated by 2 way ANOVA analysis. **(F)** Representative images of RNF213 localizing to inclusions of WT Ct, *garD*::GII, and *cdu1*::GII strains during infection of A549 cells primed with IFNγ (100 U/mL). **(G)** Quantification of RNF213 localizing to Ct inclusions during infection of unprimed and IFNγ-primed (100 U/mL) A549 cells at 24 hours post infection. Plot reflects inclusion counts across 6 fields and 3 independent biological replicates.

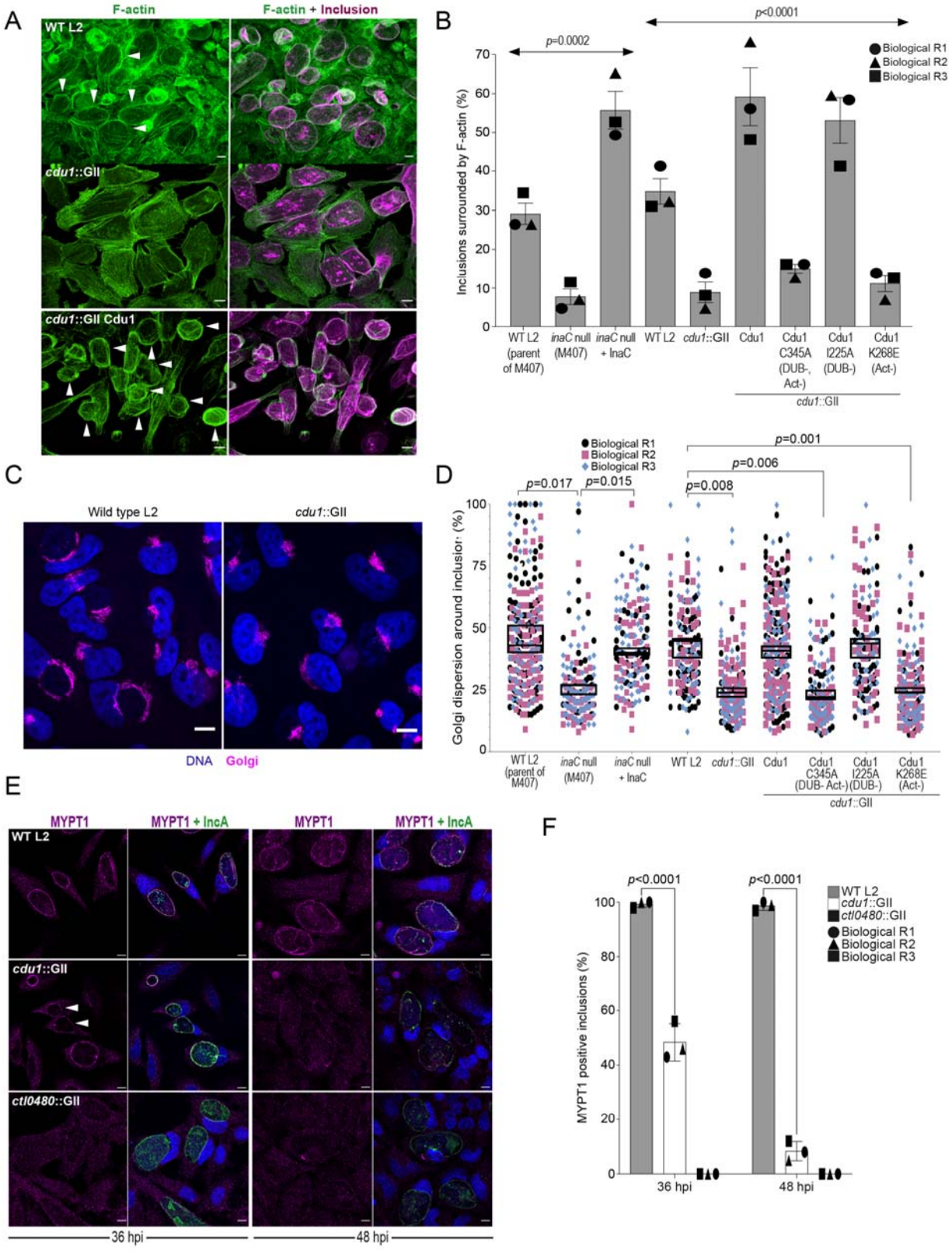

Figure 6

Cdu1 is required for assembly of F-actin, Golgi ministack repositioning, and MYPT1 recruitment to the inclusion.

(A) Examples of representative images of F-actin (arrowheads) (green, Alexa Fluor™ Phalloidin) assembled around the Ct inclusion (magenta, anti Cdu1 and Cap1 staining) in HeLa cells infected for 40 hours. Representative images for each strain analyzed can be found in Supplemental Figure 7. **(B)** Quantification of Ct inclusion surrounded by F-actin normalized to the total number of inclusions analyzed during infection of Hela cells at 40 hpi. Quantification of surrounding F-actin were obtained from inclusions imaged in 6 fields across 3 independent biological replicates. *p* values were determined by one-way ANOVAs with a Student-Newman-Keuls post hoc test. Strains used: WT L2 (Rif-R 434 Bu, parent of M407), M407 (*inaC* null strain) p2TK2, M407 p2TK2-InaC, WT L2 (434 Bu) pBOMB, *cdu1*::GII pBOMB, *cdu1*::GII pBOMB-Cdu1 Flag, *cdu1*::GII pBOMB-Cdu1^{C345A} Flag, *cdu1*::GII pBOMB-Cdu1^{I225A} Flag, and *cdu1*::GII pBOMB-Cdu1^{K268E} Flag. **(C)** Sample representative images of Golgi (anti GM130 staining, magenta) around Ct inclusions in HeLa cells infected for 24 hours. Representative images for each strain analyzed can be found in Supplemental Figure 8. **(D)** Quantification of Golgi dispersal around the Ct inclusion during infection of Hela cells for 24 hpi. The length of Golgi dispersed around each Ct inclusion imaged was measured and normalized to the perimeter length of each inclusion (% Golgi dispersion around the inclusion). Golgi dispersal around Ct inclusions was quantified from inclusions imaged in 6 fields across 3 independent biological replicates. *p* values were determined by a student paired t-test. Strains analyzed were the same ones as mentioned in (B). **(E)** Representative images of MYPT1 (magenta) at Ct inclusions (green, anti-IncA staining). Arrowheads represent *cdu1* null inclusions with low MYPT1 signal. DNA stained with Hoechst is shown in blue in panels C and E. Scale bar: 10µm. **(F)** Quantification of MYPT1 at Ct inclusions as shown in (E). Representative images in (E) and quantification of MYPT1 recruitment in (F) were obtained from inclusions imaged in 6 fields across 3 independent replicates. *p* values were determined by a student paired t-test.

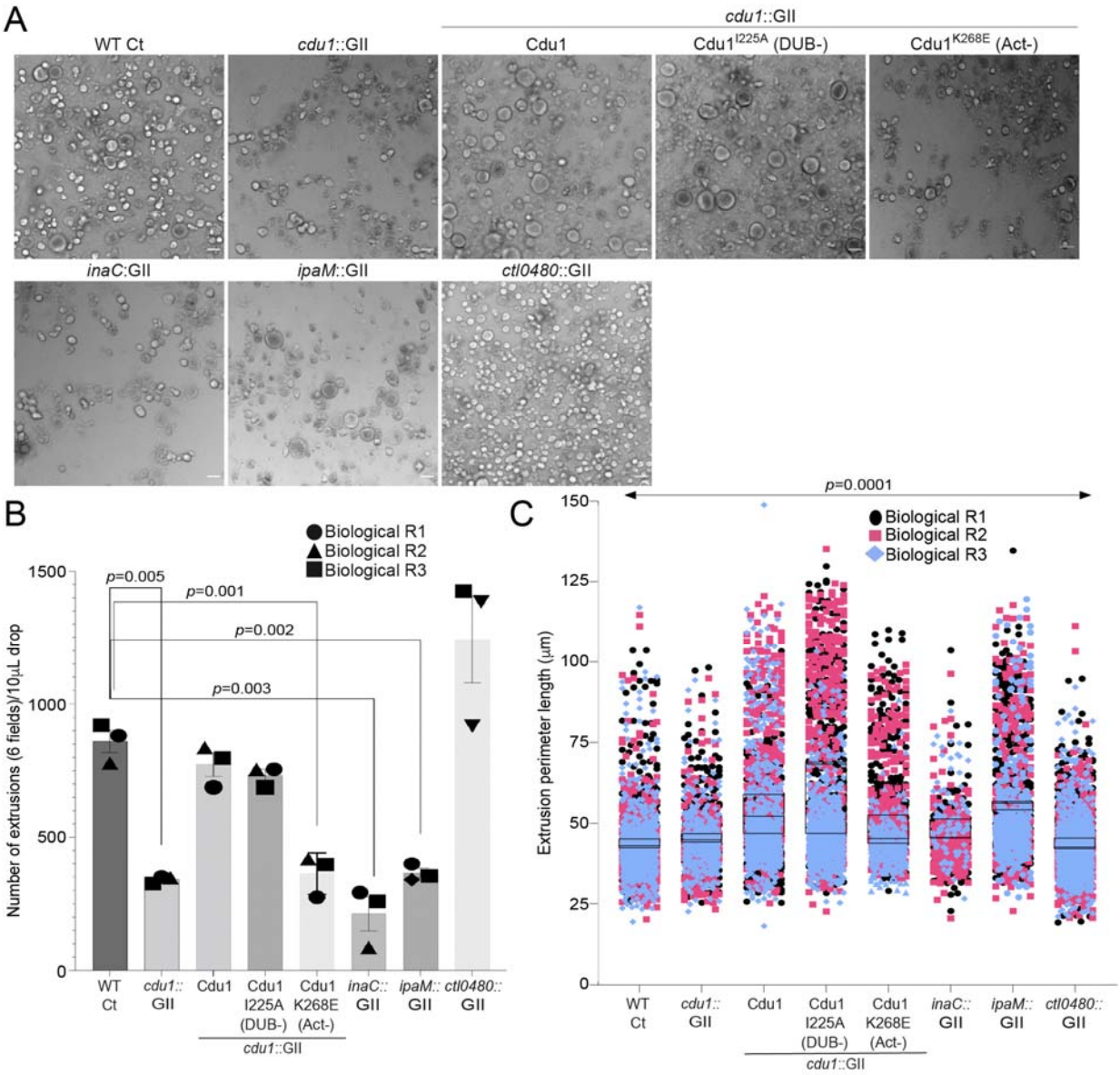

Figure 7

Cdu1, InaC, and IpaM are required for optimal extrusion of Ct inclusions from HeLa cells. **(A)** Representative images of extrusions isolated from HeLa cell monolayers infected with Ct strains for 52 hours. Scale bar: 200 µm **(B)** Quantification of the number of extruded inclusions produced by infected HeLa cell monolayers. *p* values were determined by a student paired t-test. **(C)** Quantification of the size of extruded inclusions quantified in (B). Extruded inclusions varied in size among cells infected with wild type L2 (average :43 µm), *ipaM* mutants (average: 56 µm) and *cdu1* mutants complemented wild type Cdu1 (average: 52 µm) and Cdu1^{I225A} (DUB-) (average: 60 µm). *p* values were determined by one-way ANOVAs with a Student-Newman-Keuls post hoc test. Representative images in (A) and quantification of extrusion number in (B) and extrusion size in (C) are based on images obtained from 6 fields across 3 independent biological replicates.

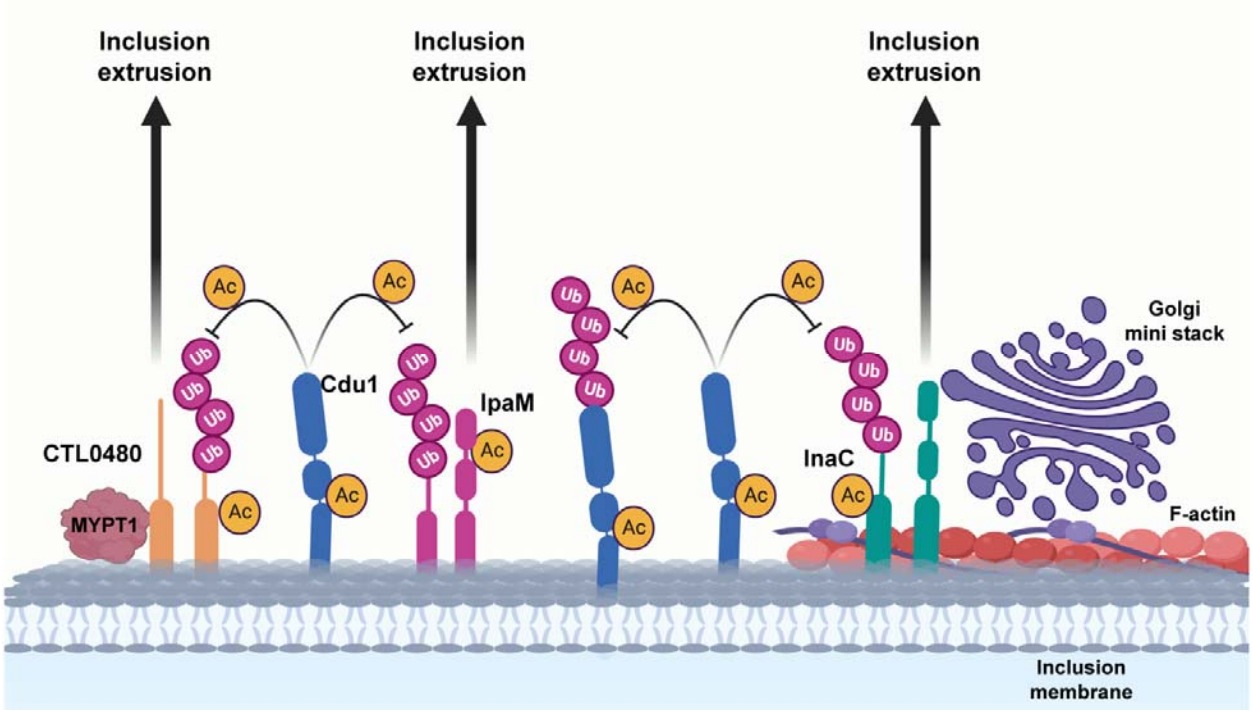

Figure 8.
A model for acetylation mediated protection of the Inc proteins InaC, IpaM, and Ctl0480 from degradation.
The cellular Ub machinery targets *C. trachomatis* effectors, including the Inc proteins InaC, IpaM, and CTL0480 for ubiquitination and subsequent protein degradation. *C. trachomatis* counters such defense mechanisms by translocating Cdu1 which protect itself and all three Inc proteins from being targeted for ubiquitination and degradation through its acetylase activity. Cdu1 protects InaC and enables the recruitment of F-actin scaffolds and Golgi ministacks to the inclusion perimeter and CTL0480 to recruit the Myosin II regulator MYPT1. All three inclusion proteins and Cdu1 promote extrusion and dissemination of *C. trachomatis* inclusions late in infection. Image generated with BioRender.com.

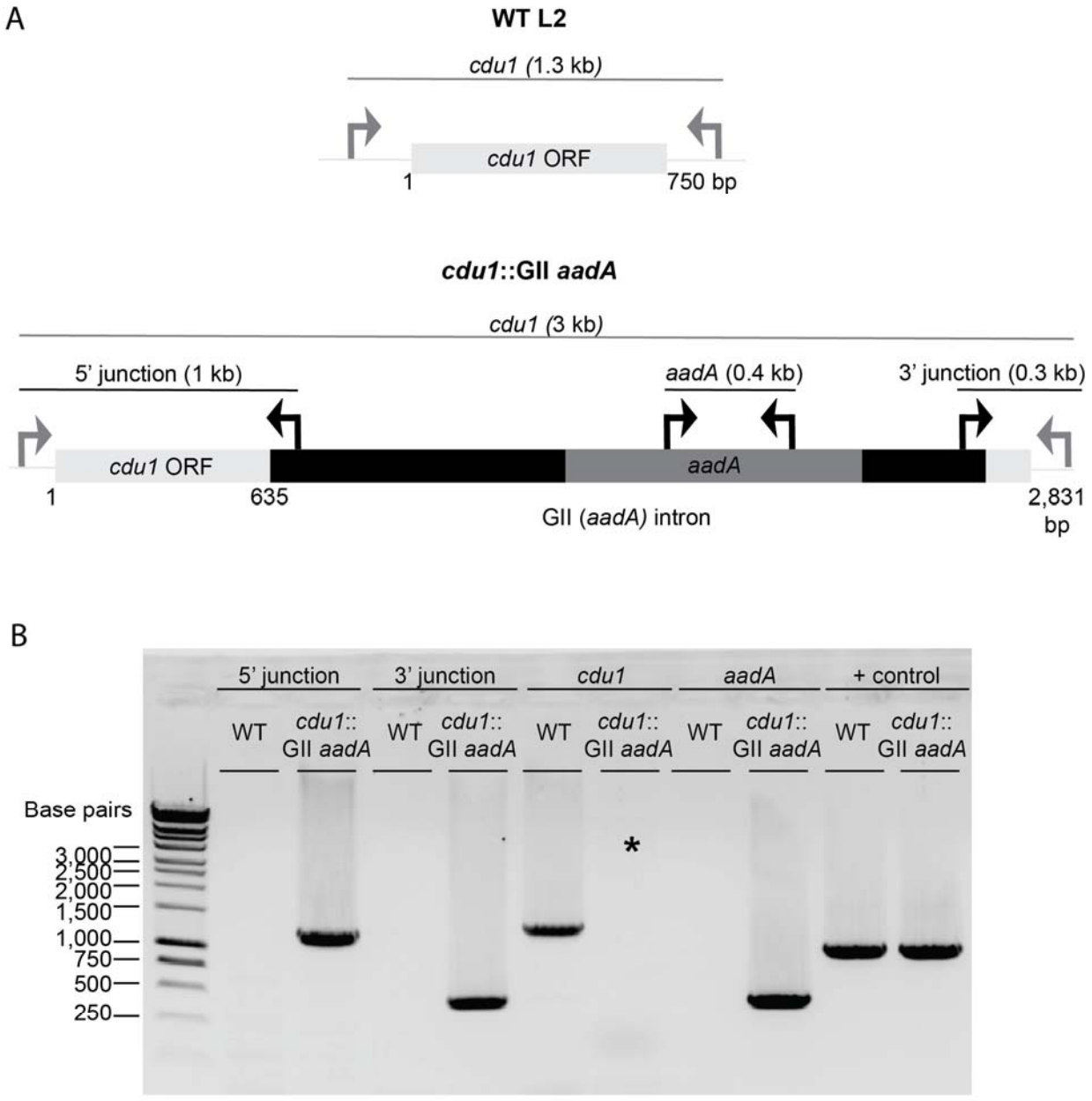

Supplemental Figure 1
TargeTron mediated disruption of the L2 *cdu1* ORF. (**A**) Depiction of the *cdu1* ORFs in WT L2 and *cdu1*::GII strains with corresponding diagnostic PCR amplicons. (**B**) PCR analysis of the disrupted *cdu1* ORF in the *cdu1*::GII strain. *Amplification of *cdu1* ORF in *cdu1*::GII strain was unsuccessful due to size of amplicon. + control: WT *cdu2*.

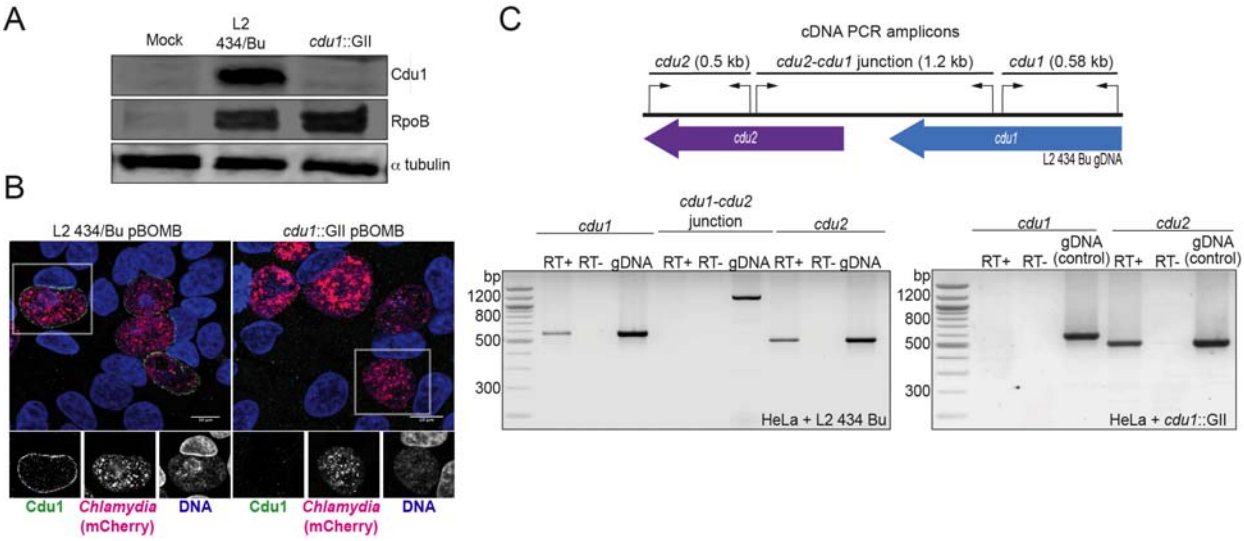

Supplemental Figure 2

Generation of a *cdu1* null strain in *C. trachomatis* (L2). (**A**) Western blot analysis of protein lysates derived from HeLa cells infected with a Ct L2 434 Bu parental strain (L2) and an L2 *cdu1*::GII *aadA* (*cdu1*::GII) strain for 24 hours. Blots were probed with antibodies raised against recombinant Cdu1 (amino acids 71-401), Ct RpoB (bacterial RNA polymerase), and human α tubulin. (**B**) HeLa cells infected with L2 transformed with pBOMB4-MCI empty vector (L2 pBOMB) and *cdu1*::GII transformed with empty pBOMB4-MCI (*cdu1*::GII pBOMB) were fixed at 24 hpi and stained with Cdu1 antisera. Cdu1 signal is depicted in green, Ct cells expressing mCherry (encoded in pBOMB4-MCI vector) are shown in red, and DNA stained with Hoechst in blue. Scale bar: 10μm. (**C**) Total RNA isolated from HeLa cells infected with L2 and *cdu1*::GII strains for 24 hours was used to synthesize cDNAs which served as templates for PCR analysis of *cdu1*, *cdu2*, and *cdu1-cdu2* bicistronic expression. RT+: Total RNA + reverse transcriptase. RT-: Total RNA without reverse transcriptase. gDNA: Genomic DNA.

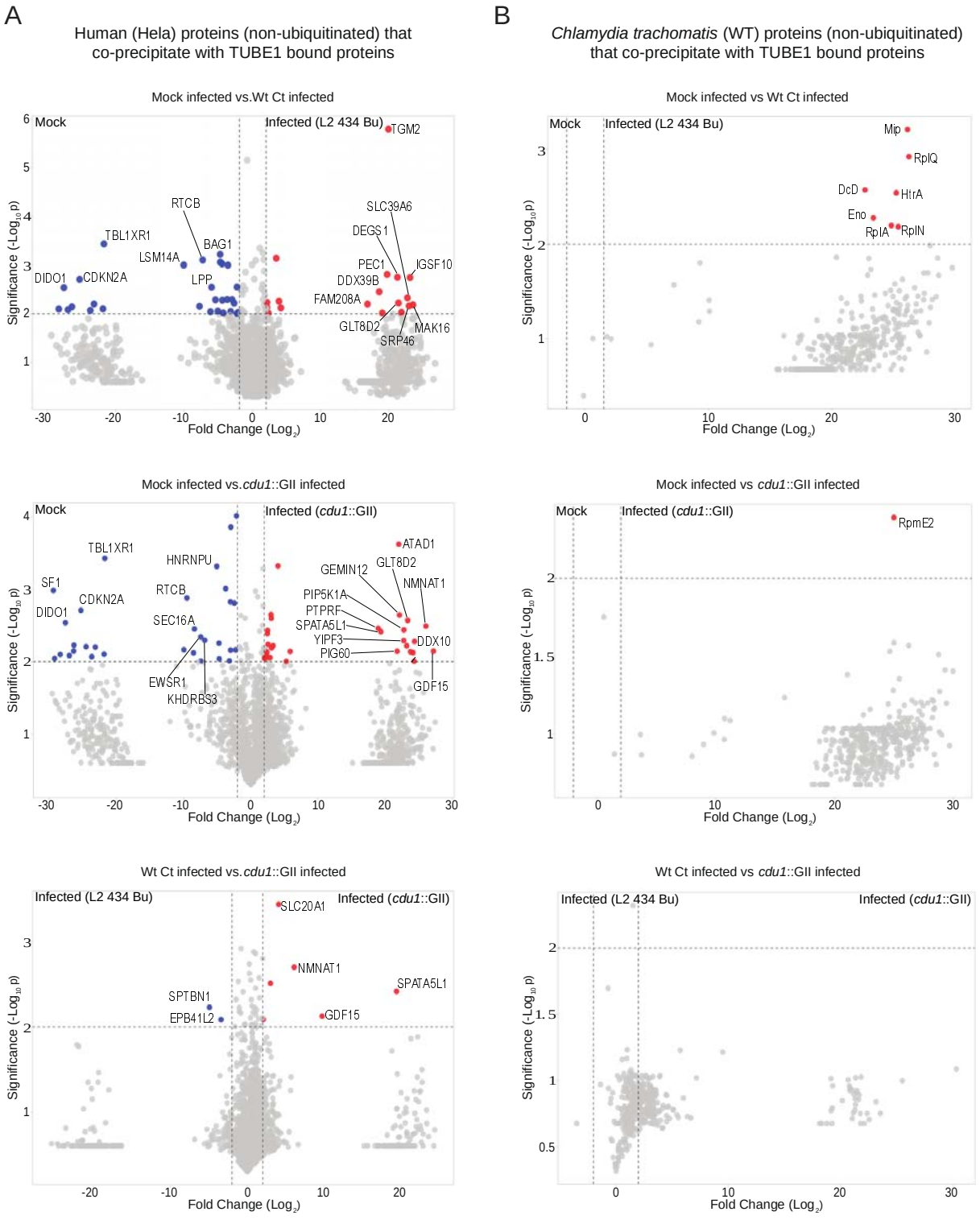

Supplemental Figure 3

Proteins co-precipitating (non ubiquitinated) with human and Ct proteins enriched by TUBE 1 pulldowns. (A) Volcano plots (pairwise comparisons) of human proteins (non-ubiquitinated) that co-precipitate with TUBE1 bound proteins in mock infected HeLa cells and HeLa cells infected with L2 or *cdu1* null strains (24 hpi). **(B)** Volcano plots (pairwise

comparisons) of Ct TUBE1 co-precipitating proteins (non-ubiquitinated) identified in mock infected HeLa cells and HeLa cells infected with L2 or *cdu1* null strains (24 hpi).

A

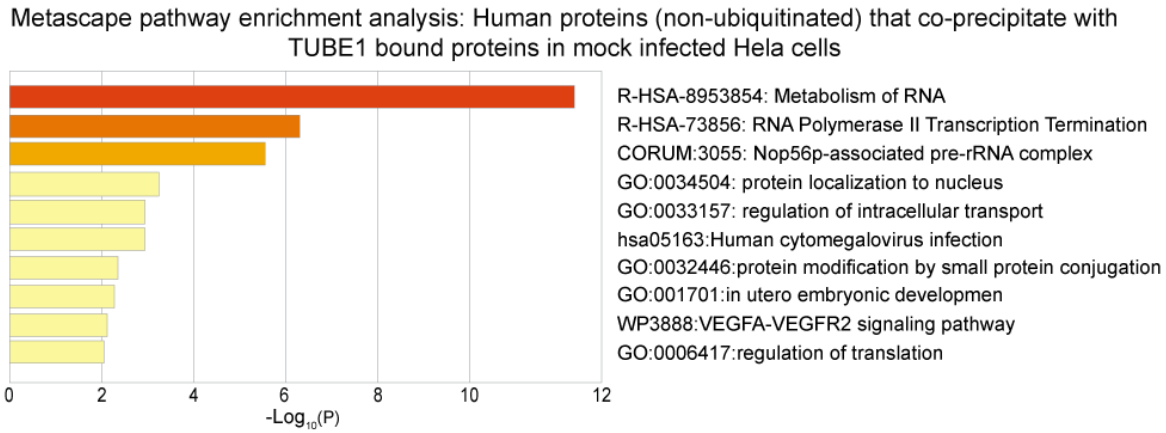

B

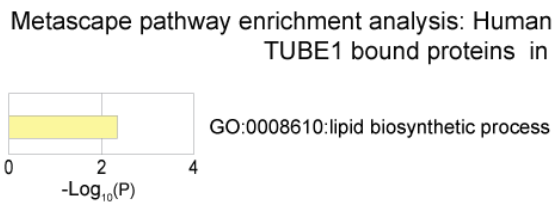

C

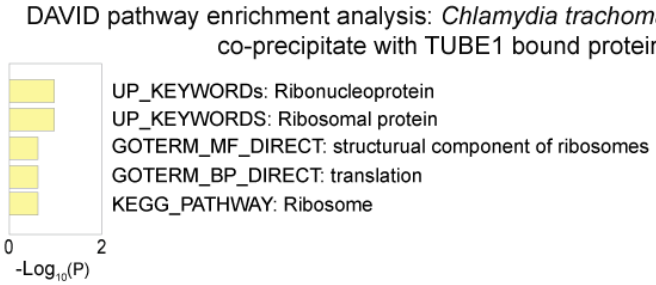

Supplemental Figure 4
Pathway enrichment analysis of human and Ct proteins that co-precipitate (non ubiquitinated) with TUBE1 bound proteins. (A) Metascape functional enrichment analysis of human co-precipitating proteins in mock infected HeLa cells. **(B)** Metascape functional enrichment analysis of human co-precipitating proteins in *cdu1* null infected HeLa cells. **(C)** DAVID pathway enrichment analysis of Ct co-precipitating proteins enriched in infected (L2 and *cdu1* null) HeLa cells.

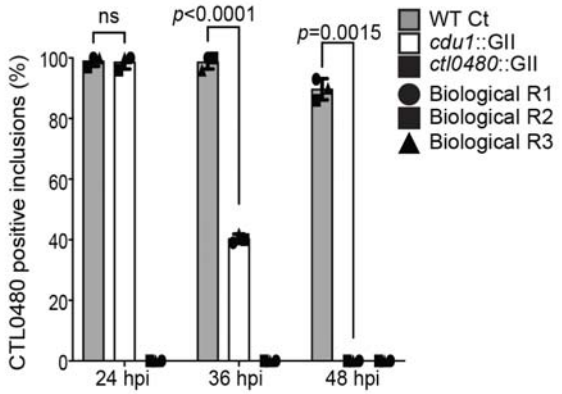

Supplemental Figure 5

Quantification of CTL0480 at Ct inclusion membranes.

Quantification of CTL0480 localization at Ct inclusion membranes as shown in Figure 3E. CTL0480 fluorescent signal was used to determine the percent of inclusions displaying CTL0480 at the inclusion membranes. Representative images and quantification of CTL0480 positive inclusions are derived from Ct inclusions imaged in 10 fields across 3 independent biological replicates. *p* values were determined by a student paired t-test.

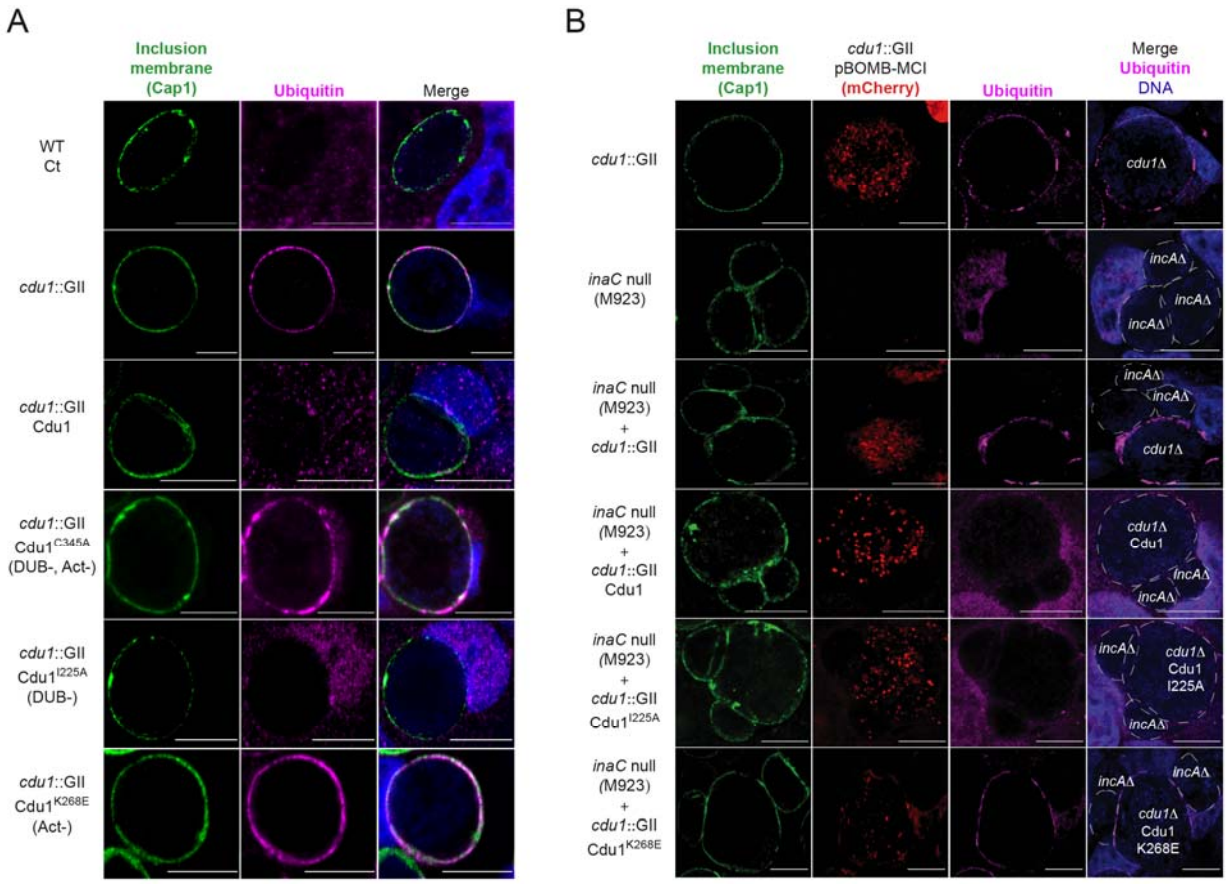

Supplemental Figure 6.
The Acetylase activity of Cdu1 is the predominant activity of Cdu1 responsible for protecting Ct inclusions from ubiquitination.
(A) Representative images of Ct inclusions (green, Cap1) decorated with Ubiquitin (magenta, FK2 antibody) in HeLa cells infected for 24 hours. Strains used: WT Ct (L2 434 Bu), cdu1::GII pBOMB MCI, *cdu1*::GII pBOMB MCI-Cdu1 Flag, *cdu1*::GII pBOMB MCI-Cdu1^{C345A} Flag, *cdu1*::GII pBOMB MCI-Cdu1^{I225A} Flag, and *cdu1*::GII pBOMB MCI-Cdu1^{K268E} Flag. **(B)** Representative images of Hela cells co-infected with an *incA* null strain and *cdu1*::GII strains expressing Cdu1 variants for 24 hours. Strains used: *cdu1*::GII pBOMB MCI, *inaC* null (M923), *cdu1*::GII pBOMB MCI-Cdu1 Flag, *cdu1*::GII pBOMB MCI-Cdu1^{C345A} Flag, *cdu1*::GII pBOMB MCI-Cdu1^{I225A} Flag, and *cdu1*::GII pBOMB MCI-Cdu1^{K268E} Flag. DNA stained with Hoechst is shown in blue. Scale bar: 10µm. MCI= mCherry.

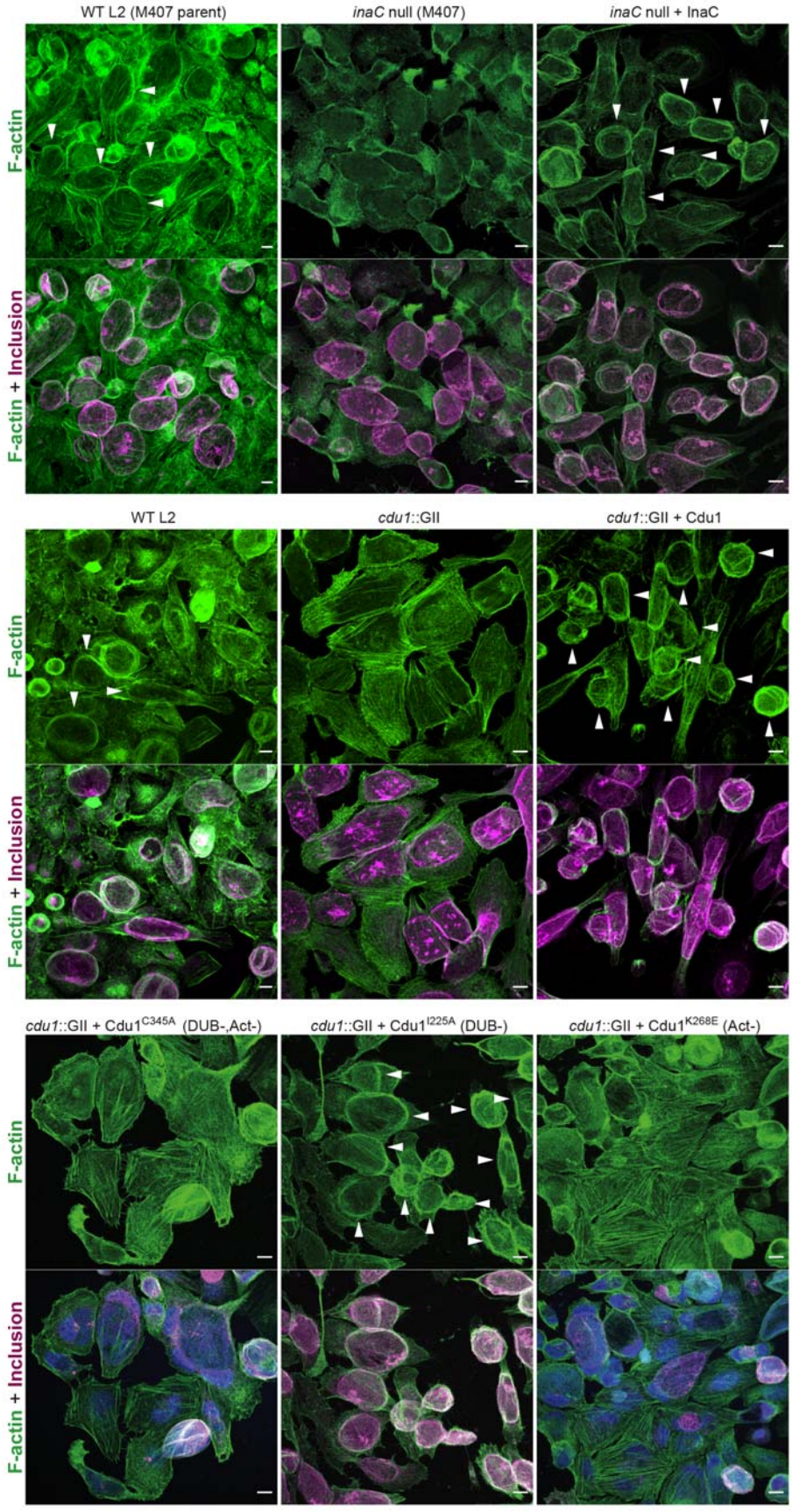

1627

Supplemental Figure 7

The DUB activity of Cdu1 is not required for assembly of F-actin around the Ct inclusion. Representative images of F-actin (arrowheads) (green, Alexa Fluor™ Phalloidin) assembled around the Ct inclusion (magenta, anti Cdu1 and Cap1 staining) in HeLa cells infected for 40 hours. Strains used: WT L2 (Rif-R 434 Bu, parent of M407), M407 (*inaC* null strain) p2TK2, M407 p2TK2-InaC, WT L2 (434 Bu) pBOMB, *cdu1*::GII pBOMB, *cdu1*::GII pBOMB-Cdu1 Flag, *cdu1*::GII pBOMB-Cdu1^{C345A} Flag, *cdu1*::GII pBOMB-Cdu1^{I225A} Flag, and *cdu1*::GII pBOMB-Cdu1^{K268E} Flag. DNA stained with Hoechst is shown in blue. Scale bar: 10µm.

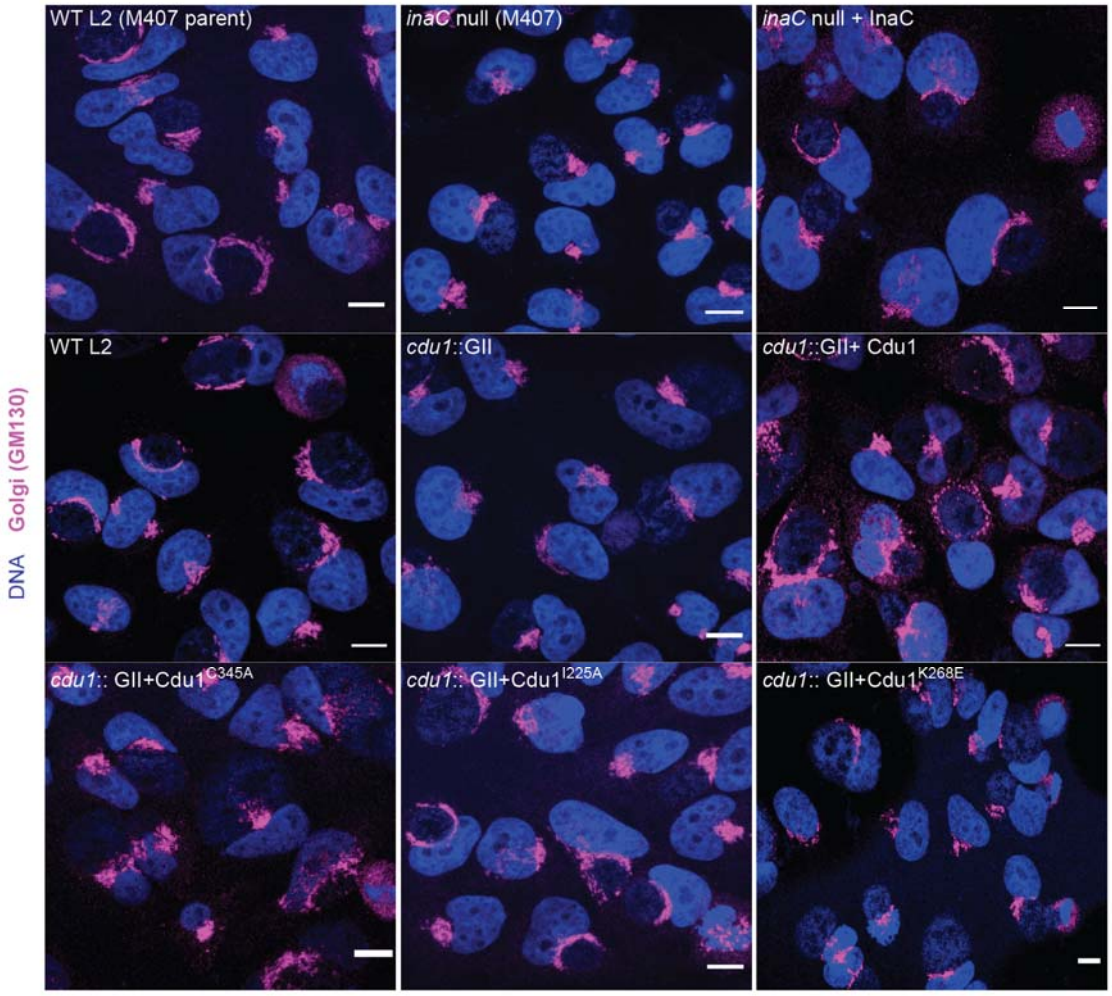

Supplemental Figure 8

The DUB activity of Cdu1 is not required for Golgi ministack repositioning around the Ct inclusion.

Representative images of Golgi (anti GM130 staining, magenta) around Ct inclusions in HeLa cells infected for 24 hours. Strains used: WT L2 (Rif-R 434 Bu, parent of M407), M407 (*inaC* null strain) p2TK2, M407 p2TK2-InaC, WT L2 (434 Bu) pBOMB, *cdu1*::GII pBOMB, *cdu1*::GII pBOMB-Cdu1 Flag, *cdu1*::GII pBOMB-Cdu1^{C345A} Flag, *cdu1*::GII pBOMB-Cdu1^{I225A} Flag, and *cdu1*::GII pBOMB-Cdu1^{K268E} Flag. DNA stained with Hoechst is shown in blue. Scale bar: 10µm.

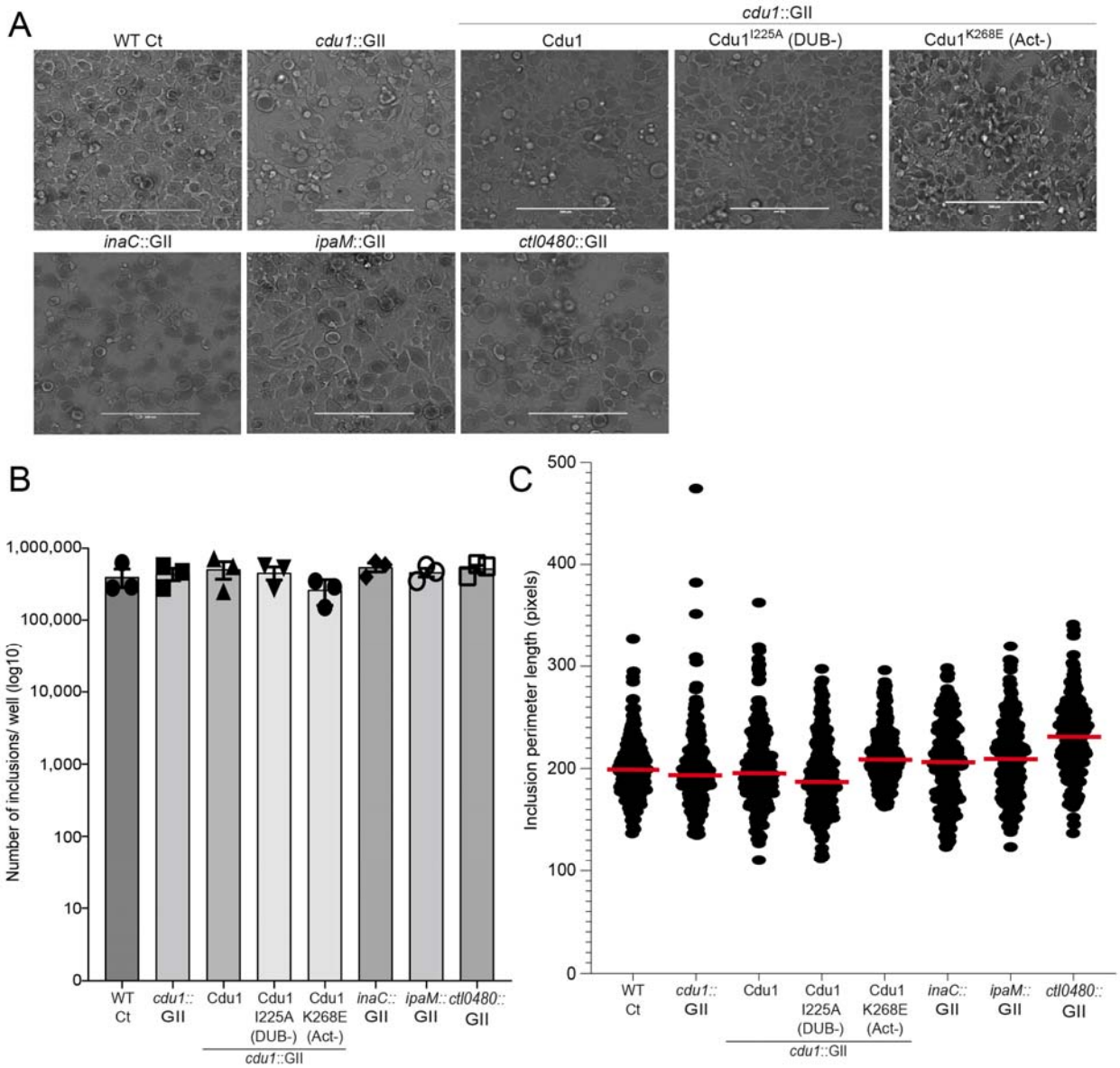

Supplemental Figure 9

The number of inclusions and the size of inclusions in *cdu1* null, *inaC* null, *ipaM* null, and *ctl0480* null strains are similar across each strain (A) Representative images of inclusions in infected HeLa cell monolayers at 48 hpi. Scale bar: 200 μm **(B)** Quantification of the number of inclusions in infected HeLa cell monolayers. **(C)** Quantification of inclusion size.